BOILING HEAT TRANSFER DURING COOLING OF A HOT MOVING STEEL PLATE BY MULTIPLE TOP JETS

by

Geoffrey Franco

B.A.Sc. (Materials Engineering), University of British Columbia, 2006

A THESIS SUBMITTED IN PARTIAL FULFILLMENT OF
THE REQUIREMENTS FOR THE DEGREE OF

MASTER OF APPLIED SCIENCE

in

THE FACULTY OF GRADUATE STUDIES

(Materials Engineering)

THE UNIVERSITY OF BRITISH COLUMBIA
(Vancouver)

December 2008

© Geoffrey Franco, 2008

ABSTRACT

Experiments have been carried out on a pilot scale run-out table to study heat transfer during cooling of hot moving steel plates. Two lines of top water jets, each holding three nozzles are used in the study. Emphasis has been placed on studying the effect of nozzle stagger, jet line spacing and plate speed on the overall heat extraction rate. Tests are performed for 3 nozzle stagger arrangements (no-, half- and full-stagger) jet line spacings (25.4 cm, and 50.8 cm) and 2 plate speeds (0.35 m/s and 1.0 m/s)

Results show that similar heat extraction rates are obtained regardless of nozzle stagger, for as long as the distance between nozzles and jet lines are held the same. However, cooling is more uniform when the nozzles are fully-staggered. No significant pooling occurred in between jet lines to affect cooling efficiency of the second jet line. More efficient heat extraction is attained when using closer-spaced jet lines and slower plate speeds.

The heat extraction capability of an individual nozzle is generally determined by the surface temperature of the to-be-impinged and surrounding areas of the steel plate to be cooled. Nozzle arrangements of subsequent jet lines with respect to hot and cold regions developed by prior jet line impingement is crucial in maintaining uniform and efficient cooling of the hot plate or strip.

TABLE OF CONTENTS

Abstract ii

Table of Contents iii

List of Tables v

List of Figures vi

Acknowledgements x

1. Introduction 1

2. Background 3

2.1. Hot-rolled Steel Production 3

2.2. Run-Out Table 4

2.3. Pool Boiling Heat Transfer 8

2.4. Jet Impingement and Hydrodynamics 11

2.5. Jet Impingement Boiling Heat Transfer 14

2.6. Previous Studies on Jet Impingement Boiling 17

2.6.1. Single-phase Forced Convection Regime 17

2.6.2. Nucleate Boiling Regime and Critical Heat Flux 18

2.6.3. Transition Boiling Regime 21

2.6.4. Leidenfrost Point and Film Boiling 23

2.6.5. Effect of Multiple Nozzles in Jet Impingement Boiling 25

2.6.6. Effect of Surface Motion on Jet Impingement Boiling 28

3. Research Objectives 34

4. Research methods 35

4.1. Experimental Procedures 35

4.1.1. Test Facility 35
4.1.2. Material and Sample Preparation 37
4.1.3. Test Matrix and Procedure 39
4.2. Analytical Procedures 43
4.2.1. Inverse Heat Conduction Analysis 43
4.2.2. Interpolation of Measured Temperature Data 49
5. Results and Discussion 53
5.1. Temperature Curves 53
5.2. Heat Flux Curves 56
5.3. Surface Contour Plots 60
5.4. Total Extracted Heat 71
5.4.1. Analysis Approach 71
5.4.2. Effect of Speed 74
5.4.3. Effect of Jet Line Spacing 76
5.4.4. Effect of Stagger 79
5.5. Temperature Gradients 81
6. Conclusion 84
6.1. Summary 84
6.2. Recommended Future Work 85
References 87

LIST OF TABLES

Table 2-1 Test conditions for experiments by Liu et al [31] 28

Table 2-2 Test conditions for experiments performed by Zumbrunnen [32] 29

Table 4-1 Summary of key specifications of pilot-scale run-out table 37

Table 4-2 Steel sample chemistry 37

Table 4-3 Test Matrix 40

Table 4-4 Mesh density information and size of elements 45

Table 4-5 Material properties of steel used in IHC model 46

LIST OF FIGURES

Figure 2-1 Schematic of a run-out table (modified from [5]) 5

Figure 2-2 Three different cooling systems (modified from [5]) 6

Figure 2-3 Schematic of pool boiling curve (modified from [13]) 9

Figure 2-4 Different types of jet impingement (modified from [13]) 12

Figure 2-5 Pressure and velocity profile, and flow regions for a jet with a uniform velocity profile (modified from [13]) 14

Figure 2-6 Jet impingement surface (modified from [9]) 15

Figure 2-7 Boiling curve for free surface jet impingement at stagnation and at 19 and 44 mm from stagnation [14] (reproduced with permission from Elsevier) 16

Figure 2-8 Jet impingement boiling curves at varying distances from stagnation [14] (reproduced with permission from Elsevier) 20

Figure 2-9 Expansion of transition boiling regime during jet impingement boiling (modified from [21]) 22

Figure 2-10 Effect of ΔT_{sub} (a) and jet velocity V_n (b) on the Leidenfrost point (modified from [23]) 24

Figure 2-11 Nusselt numbers from 3 experiments with different plate speeds (modified from 32) 29

Figure 2-12 Peak surface heat flux as a function of entry temperature (modified from [37]) 32

Figure 4-1 Schematic of pilot-scale run-out table at UBC 35

Figure 4-3 Cross-sectional view of thermocouple installation 39

Figure 4-4 TC configuration and expected impingement from no stagger case 41

Figure 4-5 TC configuration and expected impingement from 25.4 mm stagger case.... 41

Figure 4-6 TC configuration and expected impingement from 50.8 mm stagger case.... 42

Figure 4-7 2-D axisymmetric domain used in IHC analyses 45

Figure 4-8 Comparison of measured temperature and IHC results 50

Figure 4-9 Comparison of interpolated measured temperature and IHC results 51

Figure 4-10 Comparison of heat flux values calculated by IHC analysis with different acquisition rates 51

Figure 5-1 Measured thermal history for Test 2 (speed = 1 m/s, spacing = 25.4 cm, stagger = 0 mm) 53

Figure 5-2 Close-up of measured thermal history with starting temperature of 500 °C (Pass 3, Test 2) 54

Figure 5-3 Close-up of measured thermal history with starting temperature of 300 °C (Pass 7, Test 2) 55

Figure 5-4 Calculate surface heat flux history for Test 2 (speed = 1 m/s, spacing = 25.4 cm, stagger = 0 mm) 56

Figure 5-5 Close-up of the calculated heat flux history with starting temperature of 500 °C (Pass 3, Test 2) 57

Figure 5-6 Close-up of the calculated heat flux history with starting temperature of 300 °C (Pass 7, Test 2) 58

Figure 5-7 Plot of peak heat fluxes with respect to surface entry temperature for Test 2 (speed = 1 m/s, spacing = 25.4 cm, stagger = 0 mm) 60

Figure 5-8 Contour plot showing the surface heat flux (W/m^2) for the test with no stagger and an entry temperature of 500 °C 61

Figure 5-9 Contour plot showing the corresponding surface temperatures (°C) for the test with no stagger and an entry temperature of 500 °C 62

Figure 5-10 Contour plot showing surface heat flux (W/m^2) in a non-staggered configuration with an entry temperature of 350 °C 63

Figure 5-11 Contour plot showing surface heat flux (W/m^2) in a staggered nozzle configuration with an entry temperature of 350 °C 63

Figure 5-12 Contour plot showing surface temperature (°C) in a non-staggered nozzle configuration with an entry temperature of 350 °C 65

Figure 5-13 Contour plot showing surface temperature (°C) in a staggered nozzle configuration with an entry temperature of 350 °C 65

Figure 5-14 Contour plot showing surface heat flux (W/m^2) in a partially staggered nozzle configuration with an entry temperature of 350 °C 67

Figure 5-15 Contour plot showing surface temperature (°C) in a partially staggered nozzle configuration with an entry temperature of 350 °C 67

Figure 5-16 Peak heat flux values at different distances from stagnation as a function of entry temperature 69

Figure 5-17 Surface heat flux during one pass with coloured regions showing integration boundaries 72

Figure 5-18 Results of first integration step for all thermocouple locations 73

Figure 5-19 Total heat extracted for different plate speeds as a function of entry temperature 75

Figure 5-20 Effective heat extraction rate for different plate speeds as a function of entry temperature 76

Figure 5-21 Total heat extracted for different jet line spacings as a function of entry temperature 77

Figure 5-22 Total heat extracted per unit length of jet line spacing as a function of entry temperature 78

Figure 5-23 Total heat extracted for different nozzle stagger configurations as a function of entry temperature 80

Figure 5-24 Plot of the average post-pass temperature versus average entry temperature 81

Figure 5-25 Plot of the surface temperature standard deviation (σ_T) with respect to pass entry temperature 83

ACKNOWLEDGEMENTS

I would like to thank my supervisors, Dr. Matthias Militzer and Dr. Mary Wells. Their constant guidance and support proved invaluable in the completion of my research and studies. I would also like to thank Dr. Vladan Prodanovic for all his technical contributions to my project.

I am also grateful to Gary Lockhart and Phil Chan for helping me with my experiments, and to Ross Mcleod, David Torok and Carl Ng for their timely delivery of machined plates and other necessary materials.

I would also like to express my deepest gratitude to my parents Helen and Edward, my brother Brian, my cousin Gian and my pet Chelsea for their unwavering encouragement and love. Extended special thanks goes to all my MMAT, TEMP, WOW and KABA friends for keeping me sane all the time.

Finally, I would like to acknowledge Manny 'Pacman' Pacquiao, Dr. Jose Rizal, the Ateneo Blue Eagles, the Kababayan Filipino Students Association, and Edel Noreen Correa, who all serve as my daily inspirations.

AM†DG

1. INTRODUCTION

The last few decades have seen a marked increase in the development of advanced high strength steels (AHSS), e.g. dual phase (DP) and transformation induced plasticity (TRIP) steels. The development of these AHSS plays an important role in establishing sustainable engineering solutions. Such novel steels, for example, can substantially contribute to the continued development of better fuel-efficient vehicles by decreasing overall vehicle weight. This is made possible because AHSS have improved mechanical properties and therefore, less material or thinner gauge sheets can be used while ensuring design specifications are met.

Another industry benefiting from the development of AHSS is the energy sector. The increasing worldwide demand for energy has led to an unparalleled need to harvest and process natural gas. As a result, increasing volumes of gas are being transported by gas pipelines over greater distances. To take advantage of the economies of scale, larger diameter lines operating at higher pressure have been constructed to increase the throughput and lower the operating cost over the life of the lines[1]. To meet the demands of higher operating pressures, the design of pipelines have been modified to incorporate use of novel linepipe grades, i.e. X80 and X100.

The properties of any steel product are defined by its microstructure. The microstructure results from austenite decomposition during cooling and is dependent on a number of factors including steel chemistry and processing paths. For hot-rolled AHSS, the superior properties required for the aforementioned examples are attained through accelerated cooling on the run-out table of a hot rolling mill[2-4].

Accelerated cooling results in increasingly refined microstructures and the formation of non-ferritic transformation products, all of which can increase the strength of the steel. Strict control of volume fraction, size and distribution of these microstructure constituents is necessary in producing steel with a desired set of properties. This can be attained by careful control of run-out table cooling. Thus, a thorough understanding of the associated heat transfer processes as well as the development of accurate heat transfer models for run-out tables are crucial for producing advanced high strength steels.

The study of heat transfer processes on a full scale run-out table is deemed difficult, expensive and generally unrealistic. As such, researchers often perform smaller scale laboratory experiments, which include one or an array of water jets impinging on stationary or moving test specimens. At the Centre for Metallurgical Process Engineering (CMPE) at the University of British Columbia (UBC), an industrial pilot-scale run-out table facility has been built. This facility allows research to be conducted on the heat transfer processes that occur during real run-out table conditions. Using this facility, the effect of various parameters, including nozzle configuration, plate speed, and water temperature and flow rate, on the subsequent heat transfer can be investigated [2]. Results of these studies are used to optimize run-out table design and form an experimental database for modeling of the heat transfer processes during run-out table cooling. Coupled with microstructure models, these models can be used to predict final microstructures and establish better control during hot-rolled steel processing.

2. BACKGROUND

2.1. Hot-rolled Steel Production

The processing of hot-rolled steel can be subdivided into two stages: the slab-making and hot-rolling processes. The slab-making process is simply the production of steel slabs that will be formed into sheets or plates during hot-rolling. Depending on the steel mill, the starting raw material can be iron ore, recycled scrap steel or a mixture of both. It is during this processing stage that the chemical composition of the steel is finalized through ladle metallurgy. In modern steelmaking processes, the process ends with the continuous casting of the steel slabs.

The hot-rolling process can be further subdivided into three stages: reheating, rolling, and cooling. All three have significant influences on the final properties of the steel product. During the reheating stage, the slab is placed in a furnace and heated to 1200 – 1300 °C, such that the steel microstructure experiences a solid state phase change to austenite and dissolution of precipitates. The reheated slab is then moved to the rolling sections, where typically initial reduction of the slab is undertaken by a roughing mill followed by final reduction in the finishing mills. Besides shape reduction and shape control, the rolling stage is a thermo-mechanical controlled process that pre-conditions austenite grains by increasing the grain boundary surface area per unit volume. This will provide a higher nucleation site density for the subsequent austenite to ferrite transformation, resulting in a finer ferrite microstructure and a product with higher strength and toughness. After passing through the finishing mills, the steel is subjected to water cooling on a run-out table.

2.2. Run-Out Table

The run-out table plays a vital role in the production of hot rolled steels. Cooling rate is the important parameter that can change during run-out table cooling. It dictates the solid state transformation behaviour of austenite into product phases that include ferrite, pearlite, bainite and martensite. Steel with ferritic-pearlitic microstructures tend to be not as strong as those with bainitic and/or martensitic microstructures. However, bainitic and martensitic microstructures tend to be brittle. To produce steel with an ideal blend of strength and ductility, a microstructure consisting of some or all of the product phases is necessary in the final microstructure. Altering the cooling rate allows tailoring of the final phase composition and subsequently, the mechanical properties of the steel product. Hence, it is important to understand and control the run-out table cooling conditions. It is also important to ensure that cooling is homogeneous across the width of the steel strip to avoid unnecessary variations in microstructure, thermal stresses, and to maintain flatness of the strip.

A simple schematic of a typical run-out table layout is presented in Figure 2-1. Typically, hot-rolled steel leaves the finishing mill at temperatures in the range of 800 - 900 °C. The steel strip is then transported to the cooling section by means of motorized rollers. Cooling is accomplished by subjecting the hot-rolled steel to water via water jets, curtains, or sprays. The cooling section consists of several water banks, each housing and feeding water to its own set of headers. The water banks are mounted at the top and bottom of the rollers. There can be several headers within a water bank, each housing one or two water curtains or rows of jets or sprays. Top water banks are typically gravity-fed by water towers whereas bottom jet banks utilize pumps to direct water from

a storage tank onto the steel strip. To date, there is no formally established configuration for cooling and configurations usually vary significantly from mill to mill. Industrial run-out tables are designed taking into account other factors which may include space requirements, types of steel produced and gauge thickness.

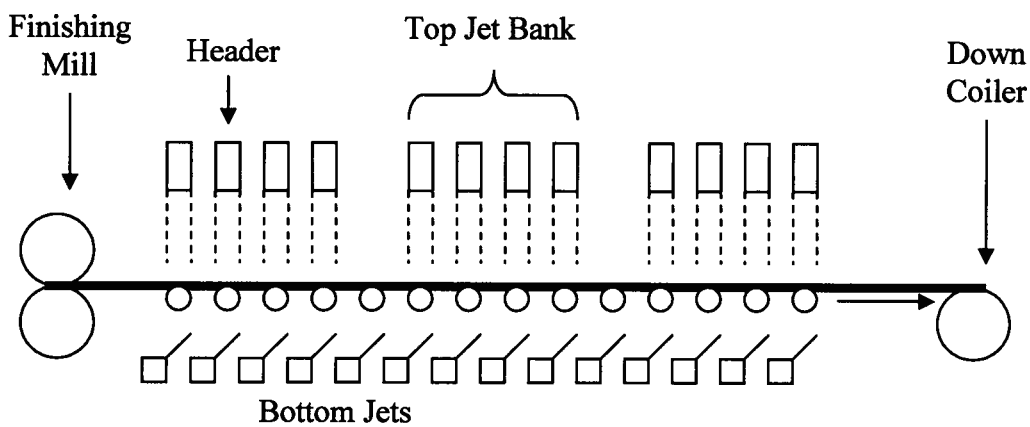

Figure 2-1 Schematic of a run-out table (modified from [5])

In industry, there are typically three different nozzle types used to provide water to the steel strip: round tube nozzles for laminar jets, slot-type nozzles for water curtains, or spray nozzles for spray cooling systems. A simple illustration of the three different systems is presented in Figure 2-2.

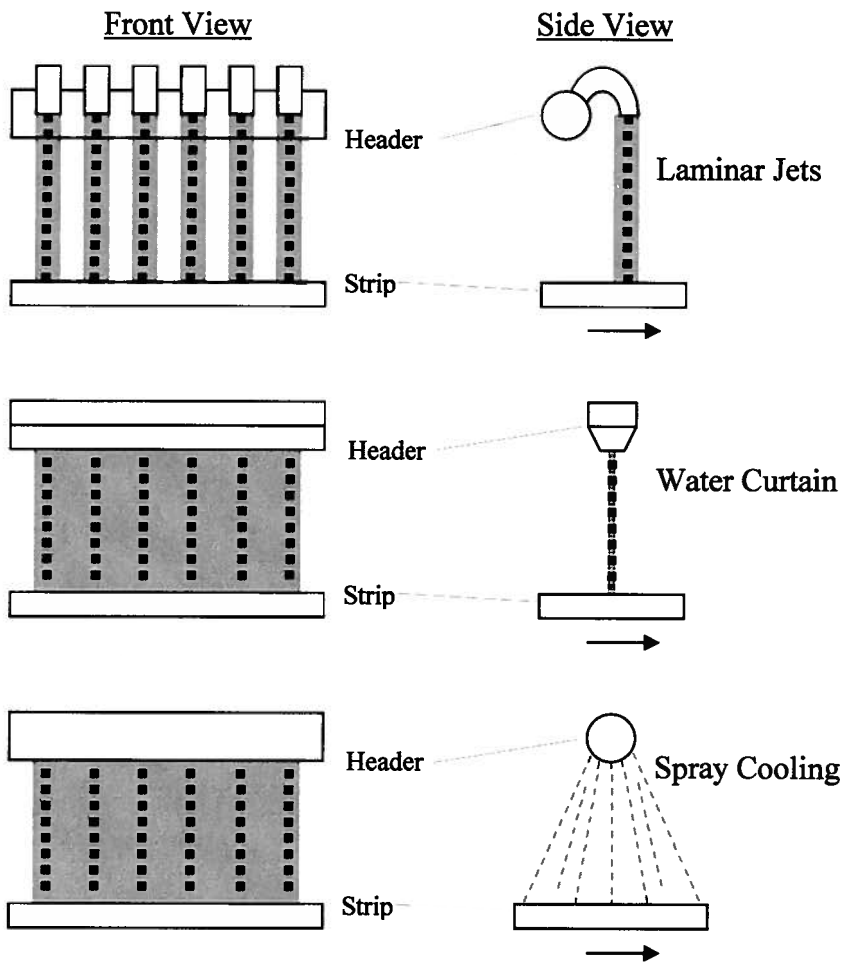

Figure 2-2 Three different cooling systems (modified from [5])

Numerous studies have been undertaken to gauge the cooling capacities of the different water delivery systems. A study done by Tacke et al.[6] found that water curtain and laminar flow systems generated higher heat transfer rates than spray cooling. An independent study by Kohrin et al.[7] verified these results by observing similar phenomena and quantifying a 10-30% improvement in cooling capacity for laminar jet cooling compared to spray cooling. It is believed that laminar jet and water curtain systems have higher cooling capacities because they allow for immediate and sustained

contact between the coolant and the hot surface, and thus a longer liquid-solid contact time[8]. Studies by Zumbrunnen et al.[9] and Chen et al.[10] reveal that uniform cooling is attained through water curtain systems since water is delivered evenly throughout the span of the heated surface. On the other hand, laminar jet systems provide more efficient cooling per unit volume of water than water curtain systems. This is due to water exiting the laminar jet nozzles with higher velocities resulting in higher heat transfer coefficients. However, since water is unevenly distributed across the span of the heated surface, the cooling attained is less uniform than in water curtain systems.

Water is used for cooling during run-out table operations because it is readily available, easy to handle and able to extract high amounts of heat from a hot surface. Its ability to extract high amounts of heat is a result of two factors. First, water has a high specific heat value and second, it has a high heat of vapourization, which allows it to further absorb more energy or heat when a phase change from liquid to vapour is involved. When the latter mechanism is involved, the underlying heat transfer that occurs is known as boiling heat transfer. This highly-efficient type of heat transfer is taken advantage of when water is used to cool surfaces that are beyond its saturation or boiling temperature. In industrial run-out tables, boiling heat transfer governs the amount and rate at which heat is extracted from the steel strip.

2.3. Pool Boiling Heat Transfer

Initial studies in boiling heat transfer were accomplished through observation of pool boiling experiments, or steady state experiments in which a pool of coolant (i.e. water) is maintained adjacent to a heated surface. The boiling phenomenon observed during run-out table cooling is certainly different in that it is highly transient in nature. However, pool boiling offers the fundamental groundwork for boiling heat transfer and much of its fundamentals can be extended to highly transient cases.

Numerous studies in pool boiling heat transfer show that there are different heat transfer mechanisms, which vary with the surface temperature. These different pool boiling regimes were first identified by Nakiyama et al.[11] and further verified by Drew and Mueller[12]. It is generally accepted that there are four distinct boiling regimes associated with boiling heat transfer. They are single-phase convection, nucleate boiling, transition boiling and film boiling [13]. To further illustrate the different regimes, a schematic of a typical pool boiling curve is presented in Figure 2-3. The pool boiling curve illustrates the surface heat flux q as a function of surface superheat, or the temperature above saturation ΔT_{sat} and specifies the different boiling regimes.

The single-phase convection regime occurs at low surface superheat. At these temperatures, the saturation temperature of the liquid has not been met and no boiling occurs. Heat transfer is generally accomplished by conduction through the water layer and supplemented by fluid motion as a result of free convection effects.

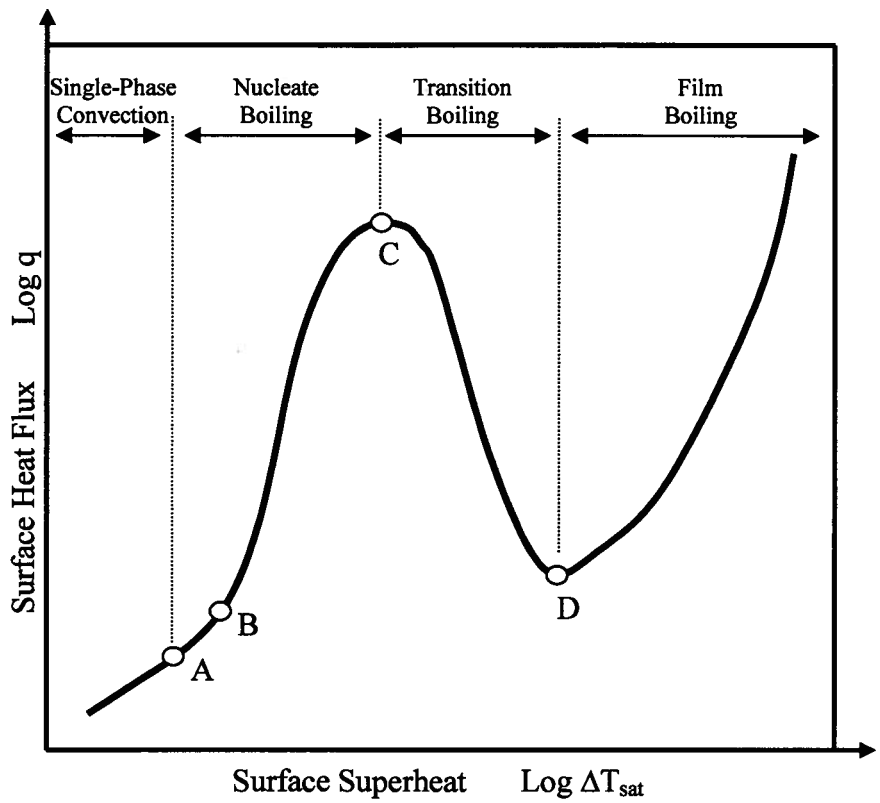

Figure 2-3 Schematic of pool boiling curve (modified from [13])

Point A demarks the onset of the nucleate boiling regime. This is often initiated a few degrees beyond the saturation temperature of the liquid as kinetic effects typically impede phase transformations at very small ΔT_{sat}. Within this regime, two different sub-regimes may be distinguished. In the region from point A to point B, isolated bubbles form at nucleation sites and detach from the surface. This separation induces fluid mixing or micro-convective effects near the surface, increasing q. This sub-regime is known as partially-developed nucleate boiling. During this sub-regime, most of the heat exchange is primarily through the liquid in motion at the surface and not necessarily through the vapor formed. As ΔT_{sat} is increased beyond point B, the sub-regime shifts from partially-developed to that of fully-developed nucleate boiling. More nucleation

sites become active and continuous inception and detachment of bubbles is sustained. As ΔT_{sat} increases, heat transfer through vapour formation improves and contributes to the rate at which q increases. However, as bubble activity and density at the surface increases, liquid motion near the surface is inhibited, decreasing contributions to q from micro-convective effects. Eventually, the overall heat flux reaches a local maximum as illustrated by point C. This point is known as the critical heat flux (CHF).

Beyond the CHF is the transition boiling regime. During this regime, considerable vapour is being formed and it begins to cover the surface. At any point on the surface, conditions may oscillate between "wet" and "dry" as the vapour blanket continues to re-form and collapse. However, with increasing ΔT_{sat}, the fraction of the surface covered by the vapour blanket increases. Since the thermal conductivity of the vapour is much less than that of the liquid, increasing ΔT_{sat} results in a continued decrease in q. As ΔT_{sat} continues to increase, contributions to q from radiation through the emerging vapour layer also increases. Eventually, the heat flux curve reaches a local minimum, shown in the figure as point D. This point of local minimum is also known as the Leidenfrost point.

Beyond the Leidenfrost point, surface heat flux starts to increase again. This point also marks the end of transition boiling and the onset of film boiling regime. During film boiling regime, the surface is completely covered by a stable vapour blanket. Heat exchange between the surface and the coolant occurs by convection of and radiation through the vapour layer. As shown below, q by radiation (q_{rad}) is a function of ΔT_{sat}:

$$q_{rad} = \sigma\varepsilon\left(T_s^2 + T_{sat}^2\right)\left(T_s + T_{sat}\right)\left(\Delta T_{sat}\right) \qquad 2\text{-}1$$

where σ is the Stefan-Boltzman constant, ε is the emissivity and T_s and T_{sat} are the surface and saturation temperatures, respectively. Hence, q continues to increase with increasing ΔT_{sat}.

2.4. Jet Impingement and Hydrodynamics

The boiling conditions during run-out table cooling are different to pool boiling since water is impinged on the surface of the hot steel strip by means of jets. In addition, the strip is moving through the water jets making the boiling condition highly transient in nature. Although similar regimes are observed as in pool boiling, the effects of jet hydrodynamics must be taken into account.

During jet impingement of a liquid on a surface, the liquid may come in contact with the surface in a number of different ways. The most common of these impingement types include free surface, plunging, submerged, confined and wall [13]. A schematic of the different impingement types are present in Figure 2-4. For run-out tables using laminar jet nozzles, only the free surface and plunging jet impingement types apply.

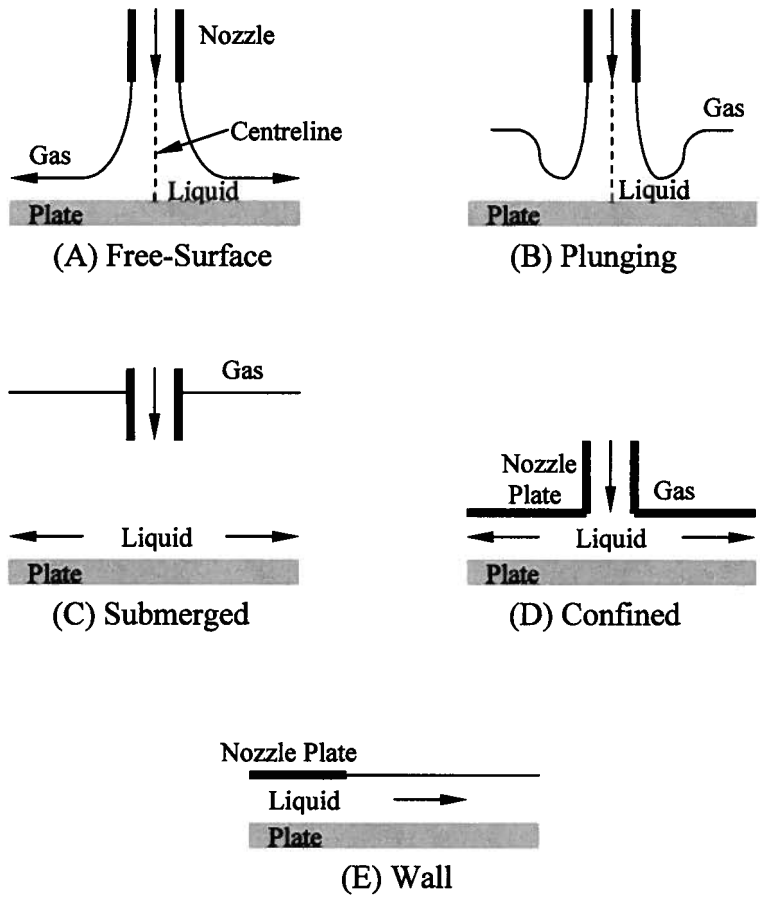

Figure 2-4 Different types of jet impingement (modified from [13])

In a free-surface impingement type, flow of the liquid from the nozzle to the surface occurs with minimal restriction. Such is the situation in run-out tables when no water has accumulated on the surface of the steel. Upon impinging the surface, the liquid traverses in a radial direction away from the point of impingement. Because the liquid is in forced motion unlike in pool boiling scenarios, heat extraction during jet impingement boiling is more efficient because of forced-convective effects. However, if the excess water is not removed and allowed to build up, the condition changes to that of plunging. In this configuration, the liquid must first penetrate and displace liquid that has built up

on the surface prior to impinging the surface. As seen in Figure 2-4, liquid movement after impingement is restricted by the surrounding build-up and this causes even more build-up surrounding the stagnation point. A plunging impingement type is known to decrease cooling efficiency as momentum is lost when displacing the liquid build-up on the surface and the forced-convective effects of jet impingement are decreased. As such, industrial run-out tables typically employ various methods of removing water between water banks to minimize pooling.

A detailed schematic of the free-surface type impingement is presented in Figure 2-5. In this case, the surface is not heated nor is it in motion. Accompanying the schematic is a plot of the pressure and velocity distribution as a function of distance along the radial direction. The impingement region (A) bounded by the diameter of the nozzle is known as the stagnation point. Pressure is highest at the stagnation point due to contributions from the jet impinging from above. Beyond this area, the liquid enters the acceleration region (B), where the liquid will accelerate until it reaches the speed of the jet flow. Beyond radial distances of twice the nozzle diameter, the fluid enters the parallel flow region (C) where the liquid traverses parallel to the surface without further acceleration.

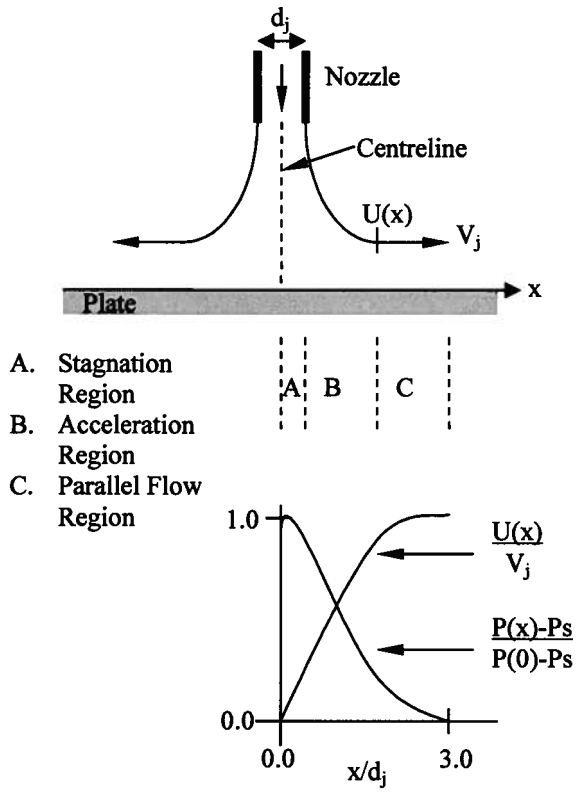

Figure 2-5 Pressure and velocity profile, and flow regions for a jet with a uniform velocity profile (modified from [13])

2.5. Jet Impingement Boiling Heat Transfer

When liquid is impinged on a heated surface, as in jet impingement boiling, the flow of the liquid is affected by the boiling phenomenon that occurs. Also, depending on surface superheat, all boiling regimes may be present during jet impingement boiling, particularly at surface temperatures beyond or around the critical heat flux. A schematic of a heated surface being impinged by a liquid is presented in Figure 2-6. This example is typical of a situation where the heated surface is at temperatures in excess of the critical heat flux.

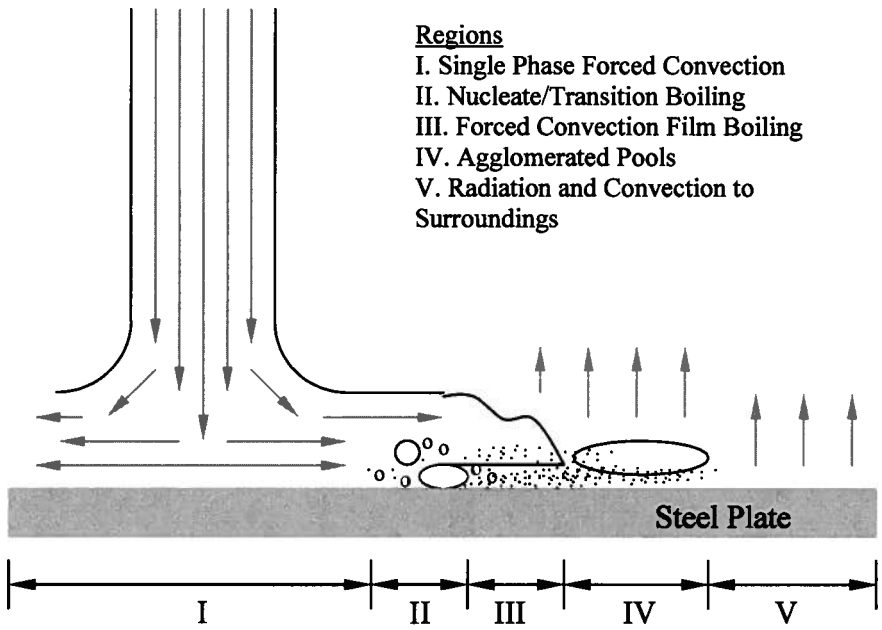

Figure 2-6 Jet impingement surface (modified from [9])

Unlike in pool boiling conditions, the added pressure from the jet flow allows the liquid to impinge and wet the surface even at higher ΔT. This immediately creates a single-phase convection region in the impingement zone (region I), and coincides with an immediate drop in local surface temperature. In the impingement zone, forced-convection effects dominate the heat transfer process, compared to free-convection effects during single phase convection in pool boiling. As such, heat extraction in the single phase regime is more efficient in jet impingement boiling and scales with ΔT, for as long as the jet is able to impinge and fully wet the surface. In the narrow annulus surrounding the single-phase convection regime (region II), both nucleate and transition boiling regimes are thought to exist. Further into the parallel flow zone (region III), bubbles begin to coalesce and form a stable vapour blanket. The region is called forced convection film boiling since the nature of jet impingement forces motion upon the liquid

and vapour layers. Further away, more of the liquid evaporates and the water layer is first reduced to agglomerated pools before ultimately evaporating completely, leaving a dry surface subject to just radiation and convection heat transfer. As expected, cooling efficiency is highest under impingement or region I. This region expands radially as the rest of the surface cools, pushing the other regions outwards until they cease to exist. Eventually, at lower surface temperatures, region I will encompass the entire surface area.

An empirical boiling curve developed by Robidou et al.[14] for jet impingement boiling is presented in Figure 2-7. Although there are noticeable differences compared to the pool boiling curve presented in Figure 2-3, all four different boiling regimes are still observed in jet impingement boiling.

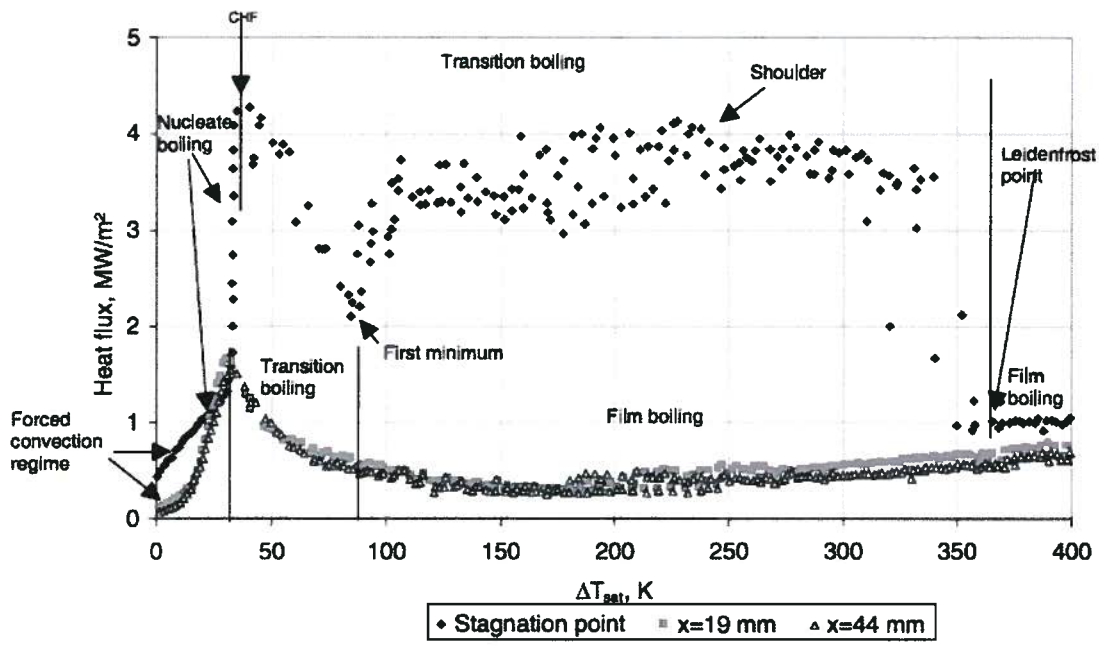

Figure 2-7 Boiling curve for free surface jet impingement at stagnation and at 19 and 44 mm from stagnation [14] (reproduced with permission from Elsevier)

Beyond surface superheat temperatures of 350 °C, only film boiling is said to be observed across the surface of the heated surface. Below superheat temperatures of 350 °C, varying locations away from the impingement zone begin to differentiate in the boiling regime experienced. Directly underneath the nozzle at the stagnation point, heat flux increases as the jet begins to break down the vapour layer. Away from this zone, the vapour layer remains stable and film boiling continues. Because of the increased heat flux in the impingement zone, temperature decreases faster in this region, ultimately wetting the surface completely as nucleate boiling and subsequently forced convection regimes take over the heat transfer process. Eventually, as the surrounding areas decrease in temperature, the vapour layer then collapses and the fully wetted zone expands.

2.6. Previous Studies on Jet Impingement Boiling

Jet impingement boiling is a highly-efficient method for extracting heat and can have numerous practical applications across many different industries. Hence, there has been much individual research emphasis on the different boiling regimes and other points of interest (i.e. CHF and Leidenfrost) occurring during jet impingement boiling.

2.6.1. Single-phase Forced Convection Regime

Investigations on the heat transfer that occurs during single-phase forced convection was carried out by Wolf et al. [15]. Their studies indicate that during the single-phase regime, the surface heat flux varies as a function of the radial distance from the stagnation point. It is proposed that the convective heat transfer coefficient is

dependent on the characteristics of the boundary layer developed, which is influenced by hydrodynamics. Beyond a certain radial distance however, the heat transfer coefficient is deemed constant as changes to the flow characteristics become negligible in the parallel flow zone. These observations were verified in studies done by Robidou et al [14]. The plot in Figure 2-7 clearly indicates that at the single-phase regime, the reported heat flux at the stagnation point is much higher than values reported at distances further away. At two different distances within the parallel zone, there is no difference in the recorded heat flux.

Another consideration is the pressure distribution over the radial distance in free-surface type jet impingement. The pressure distribution determines the local saturation conditions of the liquid along the surface. Such differentiation in saturation temperature will cause variation in liquid sub-cooling and surface superheat, and a subsequent shift in the boiling curve. Experimental work by Hauksson [16] found that the increased pressure in the stagnation point causes up to a 5 °C increase in saturation temperature.

2.6.2. Nucleate Boiling Regime and Critical Heat Flux

While jet flow hydrodynamics will have a pronounced effect on the heat flux values in the single-phase regime, Wolf et al. [15] determined that this did not occur in the nucleate boiling regime. It is surmised that during the nucleate boiling regime, heat exchange through vapour formation dominates the heat transfer process such that contributions from forced-convective effects and hydrodynamics become negligible. However, studies by Miyasaka et al. [17] found the transition to nucleate boiling from transition boiling (CHF) may shift to a higher heat flux and surface superheat with

increased jet flow velocity and larger liquid subcooling. This was verified by numerous other researchers who report a strong dependence of CHF on jet flow velocity and liquid subcooling [18-20].

Mitsutake and Monde [20] experimented with other parameters including liquid subcooling. They found that increasing the liquid subcooling tend to increase the size or radial bandwidth of the nucleate/transition boiling regime that circumcise the single-phase regime. They also found that varying the jet velocity causes the nucleate boiling annulus to traverse to a predetermined radial distance away from the stagnation point faster. Based on their observations, Mitsutake and Monde developed a relationship for the location of the boundary between the nucleate boiling regime and the single-phase regime as a function of time. The developed relationship is presented by:

$$r_{wet} = a \times t^{n} \qquad 2\text{-}2$$

where a and n are experimentally determined constants, r_{wet} represents the radius of the wetting zone, and t is the time.

The boiling conditions outside of the stagnation point during the nucleate boiling regime were also considered in the experimental work of Robidou et al[14]. A plot of the different boiling curves developed for different distances away from stagnation point is presented in Figure 2-8.

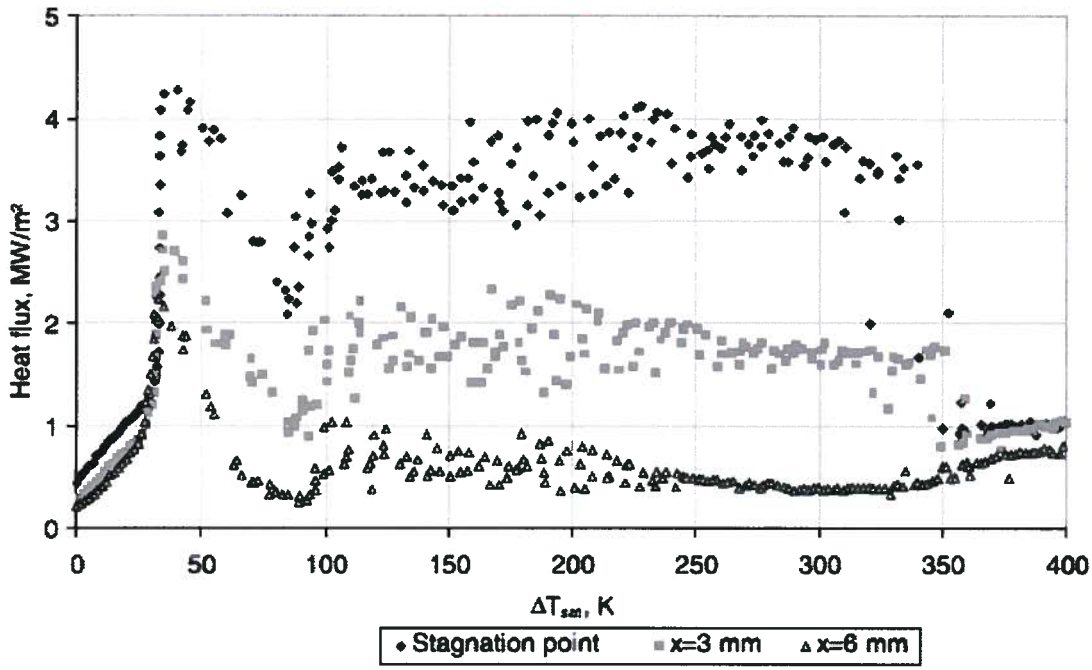

Figure 2-8 Jet impingement boiling curves at varying distances from stagnation [14] (reproduced with permission from Elsevier)

Robidou et al [14] found that the change from transition boiling to nucleate boiling away from the stagnation point occurred at lower ΔT_{sat} and are marked by lower local CHF values. However, the CHF for the locations away from stagnation tend to occur along the nucleate boiling curve developed for the stagnation point. It is believed that transition boiling persists at lower ΔT_{sat} since there is less pressure at distances away from the stagnation point. Hence, the location in the boiling curve of the CHF reflects this variation in hydrodynamics as observed by Miyasaka and others [17-20].

It can then be said that for a given set of jet impingement boiling parameters, there is a universal curve for all locations at the temperature range wherein nucleate boiling exists. This suggests that all locations will follow the same nucleate boiling curve for as long as the fluid flow conditions permit it – i.e. there is sufficient pressure from the

liquid to retard vapour formation. Increased fluid pressure will extend the nucleate boiling regime and the CHF to higher q and ΔT_{sat}. Since the fluid pressure in the parallel flow zone is less than in the stagnation zone, vapour films initiate at lower temperatures. The respective boiling curves at these locations diverge at lower CHF and ΔT_{sat}.

2.6.3. Transition Boiling Regime

In jet impingement boiling, transition boiling is thought to exist in the annulus surrounding the fully-wetted region. This thought is based on accounts that a non-uniform heat flux profile is observed within this annulus [17, 21]. Studies by Pan et al. [22] showed that unlike in nucleate boiling, hydrodynamics has a significant effect on heat flux values within the transition boiling regime. This observation is also made in the work by Robidou et al. [14]. As shown in Figure 2-8, there is a noticeable discrepancy in the transition boiling heat fluxes at varying distances from the stagnation point. These distances are also representative of the varying hydrodynamic conditions observed during jet impingement. Pan et al. mentioned that increased liquid turbulence and bubble agitation observed at the stagnation point enhances heat extraction during transition boiling. Robidou et al. explained this effect by suggesting that the process of bubbles breaking apart to smaller bubbles, or microbubble emission, is responsible for this increased liquid turbulence.

Hamad et al. [21] studied the development of the transition boiling regime using images taken during jet impingement boiling experiments. In their study, they observed discernable features that demarcate the radial edge of the wetted zone (r_w), and as well as the radial edge where no boiling occurs (r_s). They believed that these features bound the

transition boiling regime and were subsequently tracked to show its evolution. Results of their study are presented in Figure 2-9. In addition to r_s and r_w, the figure also tracks the radial position of where the maximum heat flux (r_q) and maximum heat transfer (r_h) coefficient are observed.

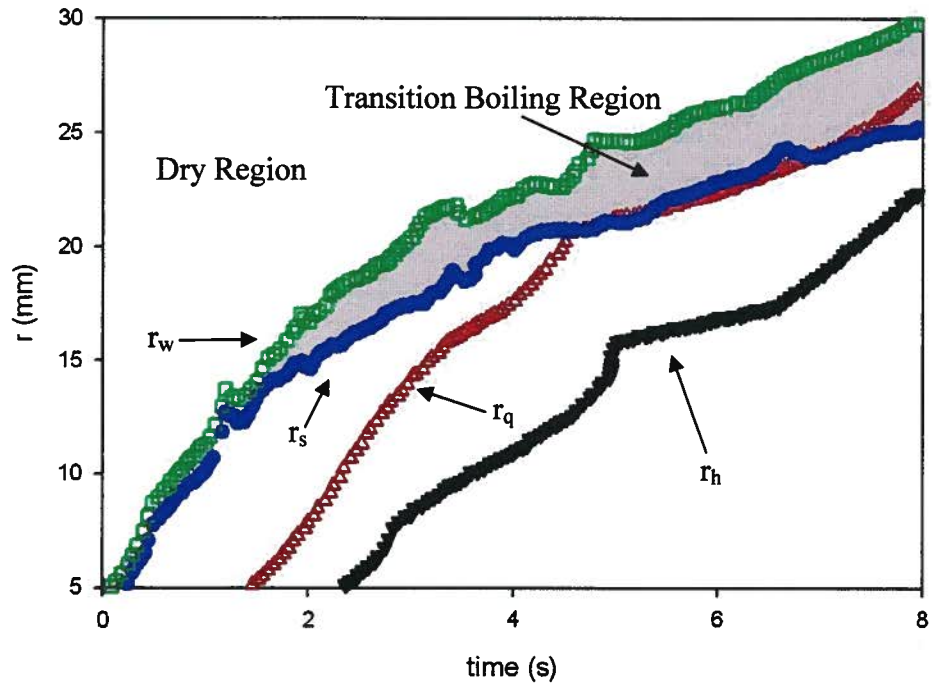

Figure 2-9 Expansion of transition boiling regime during jet impingement boiling (modified from [21])

Based on observations by Hamad et al. [21], the transition boiling regime does not emerge until one second after the plate is impinged by the jet. As r_s and r_w traverse further away from the stagnation point, the distance between them expands suggesting that the transition boiling regime also expands as it evolves. It is also worth noting that prior to the five second mark, the maximum heat flux is recorded inside the region where no boiling occurs. Thereafter, the maximum heat flux is observed at the same radial location as r_s.

2.6.4. Leidenfrost Point and Film Boiling

At the Leidenfrost point, heat flux is at its minimum and a stable film develops marking the onset of film boiling. In jet impingement boiling studies, the location of the Leidenfrost within the boiling curve is considered important since it is associated with the progression of the rewetting front. Hence, the Leidenfrost point is also referred to as the rewetting temperature.

Numerous researchers have observed that the Leidenfrost point is strongly affected by the amount of liquid subcooling ΔT_{sub}, or the temperature below saturation. Similar observations are made with regards to the effect of jet velocity [23,24]. The dependence on jet velocity is indirectly a result of liquid subcooling since the varying pressure that corresponds with jet velocity changes the saturation temperature of the liquid, and hence the liquid subcooling as well.

The effect of ΔT_{sub} and jet velocity is documented in studies by Ishigai et al. [23]. A summary of their findings is presented in Figures 2-10a and 2-10b. Figure 2-10a shows that with a larger ΔT_{sub}, the Leidenfrost point is shifted to higher heat fluxes. The same conclusion is drawn with increasing jet velocity, as shown in Figure 2-10b. However, increasing the jet velocity does not shift the Leidenfrost point to higher ΔT_{sat} as observed with larger ΔT_{sub}.

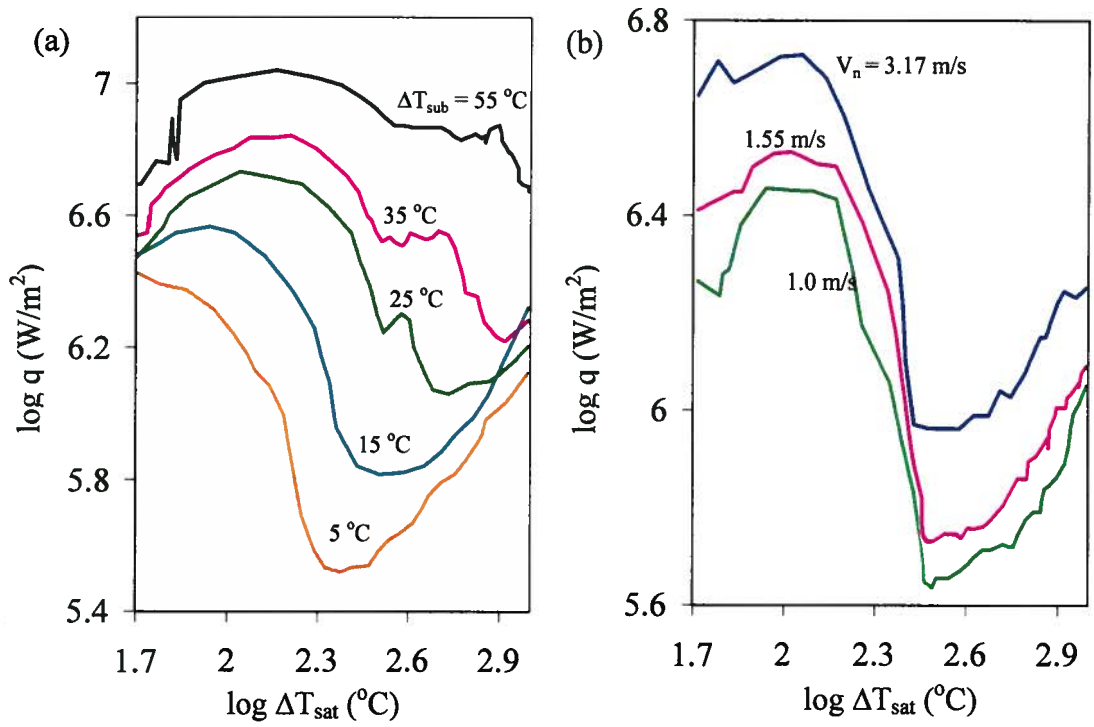

Figure 2-10 Effect of ΔT_{sub} (a) and jet velocity V_n (b) on the Leidenfrost point (modified from [23])

Based on their observations, Ishigai et al.[23] formulated a correlation to determine the heat flux at the Leidenfrost point as a function of both jet velocity v_{jet} and liquid subcooling, i.e.

$$q_{\min} = 5.4 \times (1 + 0.527 \Delta T_{sub}) \times v_{jet}^{0.607} \times 10^4 \quad (\mathrm{W/m^2}) \qquad 2\text{-}3$$

A similar study was performed by Liu [24] to develop a new correlation for the minimum heat flux which included the diameter of the nozzle. The resulting correlation from this study is given by

$$q_{\min} = 0.20 \Delta T_{sub} (v_{jet}/d)^{0.5} \times 10^4 \quad (\mathrm{W/m^2}) \qquad 2\text{-}4$$

Under the same conditions, minimum heat flux values calculated using Liu's developed relationship are found to be 20% less than those calculated using Ishigai's

equation. However, both correlations suggest a strong dependence of the minimum heat flux on ΔT_{sub}. Liu also observed that a linear relationship exists between the surface superheat temperature where the Leidenfrost point occurs and ΔT_{sub}.

Similarly, heat flux in film boiling has a strong dependence on liquid subcooling. Studies by Liu and Wang [3] suggest that liquid subcooling has a much stronger effect on heat transfer than jet velocity. In their studies, they observed that larger liquid subcooling causes the boiling curve to shift to higher surface superheat temperatures and heat flux. The same observations were made in studies by Zumbrunnen et al. [9].

The effect of distance from stagnation on the heat transfer at the Leidenfrost point and film boiling regime was studied by Robidou et al [14]. As shown in Figure 2-7, the Leidenfrost point at locations away from the stagnation occurred at much lower surface superheat temperatures. When film boiling is experienced at all locations, the heat fluxes at the stagnation zone are found to be approximately 25% higher than in the parallel flow zone. Robidou et al. believed that the film layer in the stagnation zone is thinner, giving rise to a higher thermal gradient, and subsequently heat flux than experienced in the parallel flow zone. Robidou et al. also noted that there were no observable fluctuations in temperature during film boiling, thus suggesting that the vapour layer developed is stable.

2.6.5. Effect of Multiple Nozzles in Jet Impingement Boiling

In run-out table cooling, multiple nozzles arranged in arrays are used to cool the steel strip. In laminar nozzle systems, water from a top nozzle will spread radially as shown in Figures 2-4 to 2-6. When using multiple nozzles, the spread from each nozzle may interact with one another. Such interactions further complicate the underlying heat

transfer process that occurs during run-out table cooling and many studies have been undertaken to further understanding of it.

According to Filipovic et al. [25], multiple impingements causes 3 distinct cooling regions to occur and are identified as the following:

1. The impingement cooling zone, where water from the jet immediately comes in contact and wets the surface
2. The interaction zone between two neighboring jets in the same jet line
3. The interaction zone between jets from consecutive jet lines

Monde et al. [26] studied the effects of multiple jet impingements on nucleate boiling heat transfer by utilizing combinations of 2 to 4 jets impinging on a heated surface. Heat flux values from their experiments are compared with results from earlier studies which used a single, circular, free-surface jet. They observed that the degree of scatter in the data is typical for nucleate boiling and concluded that multiple jet impingements had little to no effect on the heat flux in the nucleate boiling regime. Results of these studies are reviewed by Wolf et al. [13]. They suggested that the scatter initially observed by Monde et al. is not random. Wolf et al. showed that for comparisons with respect to position, where the number of jets is fixed, sizable and consistent differences in the heat flux are observed.

Further investigations on multiple jet impingement were carried out by Sakhuja et al. [27]. In their study, nozzles were arranged in a staggered configuration and nozzle spacing was varied and ranged from 4 to 12 nozzle diameters apart. They observed that the nucleate boiling heat flux is influence by the nozzle-to-nozzle spacing and that

maximum heat fluxes were reported when the nozzle spacing was in the range of 8 to 10 diameters apart.

Slayzak et al. [28,29] experimentally studied the interaction between two jet lines. Results of their experiments indicate that there were three high heat transfer regions along the heated sample surface. Two of these high heat transfer regions correspond to the stagnation points of the two jet lines. The third high heat transfer region occurred at the interaction zone between the two jet lines. In the experiments, the jet line spacing used was far enough apart that the median between two jet lines lies well outside of both impingement cooling zones. Despite this, the heat transfer coefficient in this area was found to be comparable to those observed in the impingement cooling zone. Slayzak et al. suggested that the high heat flux region in the interaction zone between jet lines is caused by the formation of an interaction fountain that results from the colliding flows. When the jet velocity of the jet lines were varied from one another, the location of the interaction zone shifts from the median and towards the weaker jet.

Haragushi and Harkik [30] investigated the effect of jet spacing on the uniformity of heat extraction by multiple jet lines. In their experiments, jet diameter, jetline spacing and nozzle to plate distance were held constant and the nozzle spacing within a jet line was systematically varied. They found that reducing the nozzle spacing in a jet line greatly improves the uniformity of cooling across the width of the heated sample plate. They deduced that uniform cooling is achieved if the impingement zones of the jets wholly cover the distance between nozzles.

The effect of nozzle configuration on the heat transfer occurring in the interaction zone was investigated by Liu et al. [31]. In their experimental work, two or more jets

were used and the nozzle spacing, water temperature and water flow rate were varied. A summary of their test parameters is presented in Table 2-1.

Table 2-1 Test conditions for experiments by Liu et al [31]

No. of Nozzles	Nozzle Spacing, mm	Water Temperature, °C	Flow Rate, l/min
2	140	13	58/58
2	140	27	60/60
2	140	28	30/60
2	80	28	30/30
3	90	30	30/30/30

Liu et al. concluded that jet interactions in general have significant effects on the heat transfer that occurs during jet impingement boiling. When the two flows collide, an interaction fountain is reported as similarly observed in studies by Slayzak et al. [27,28]. However, Liu et al. found that cooling intensity is weakest at the flow interaction area. It is deduced that flow at the interaction area is essentially stagnant as the flows from opposite directions cancel each other out. Thus, the local heat transfer coefficient in this area is also reduced. However, the cooling intensity at the interaction zone increases when the nozzle spacing is close enough such that the impingement zones of two neighboring jets interact with each other. When there is discrepancy between flow rates of adjacent jets, lower heat fluxes are recorded by the weaker jet as the crossflow imposed by the stronger jet produces less favourable hydrodynamic conditions.

2.6.6. Effect of Surface Motion on Jet Impingement Boiling

Jet impingement boiling during run-out table cooling is further complicated by movement of the steel strip. In stationary surfaces, the impingement zone created by

circular nozzles is typically circular in shape. This is not necessarily the case when motion is incorporated. Also, unlike for stationary surfaces where the impinged area remains the same, movement of the surface only allows limited contact time between the jet and the impinged area.

Zumbrunnen et al. [9, 32] studied the effects of motion during jet impingement of a heated surface. A summary of the different parameters tested is presented in Table 2-2, and results of their study are shown in Figure 2-11.

Table 2-2 Test conditions for experiments performed by Zumbrunnen [32]

Test Speed	Reynold's number	Jet Velocity (m/s)	Jet Width (mm)	Initial Plate Temperature (°C)	Water Temperature (°C)
0 m/s	24000	2.60	1.02	95	21.2
0.15 m/s	24000	2.60	1.02	106	22.9
0.31 m/s	24000	2.60	1.02	92	21.3

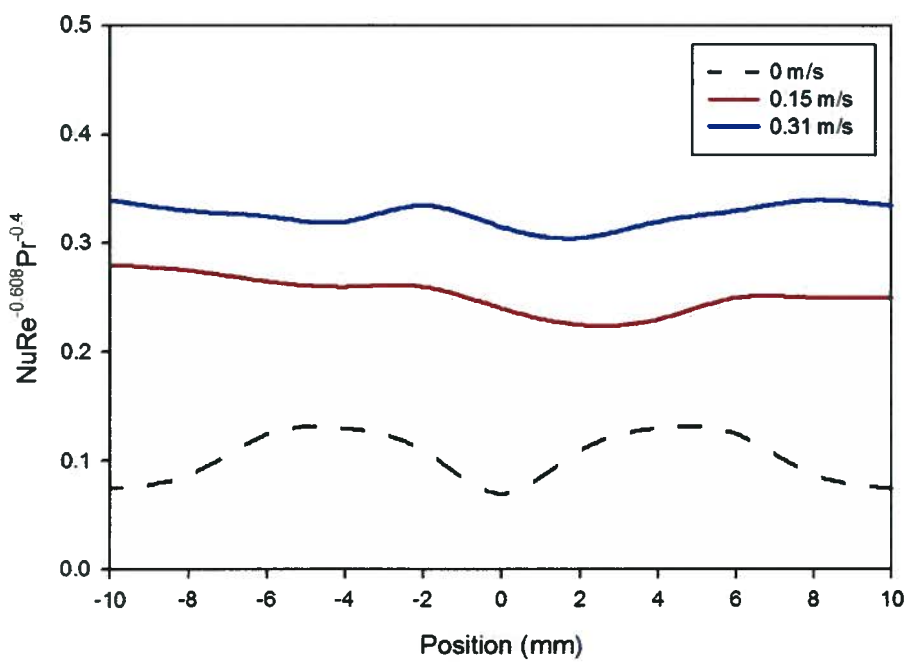

Figure 2-11 Nusselt numbers from 3 experiments with different plate speeds (modified from 32)

In the study, the heat and mass transfer distributions for a moving flat surface are estimated through numerical analyses utilizing the Navier-Stokes equation. In these estimations, both the effects of surface temperature and surface motion were considered. Because the same fluid make-up (water) and velocity are used in the tests, the same Reynolds (Re) and Prandtl (Pr) number are constant for all experiments. Hence, the plot shown in Figure 2-11 shows the variation in Nusslet number (Nu) as a result of different test speeds. Their experimental work shows that a moving surface causes the Nu to increase. Nu is a dimensionless value that describes the relationship between the convective heat transfer that occurs, and the conductive heat transfer that would have occurred had there been motionless fluid instead. Hence, a larger Nu would correspond to larger heat fluxes and greater cooling capacities. Zumbrunnen et al. believe that the larger Nu reported for moving surfaces is a result of increased turbulence in the boundary layer. This subsequently improves heat transfer. They also suggest that in a stationary surface set-up, a more stagnant and thicker boundary layer develops resulting in less heat transfer.

The effect of varying surface velocities was investigated by Hatta et al. [33]. In their experimental work, a moving hot steel plate was passed under a laminar water curtain at different velocities. The velocity of the sample plate was systematically varied between 0.48 and 2.4 m/min. Their studies show that the sample plate's velocity has a strong effect on the cooling that takes place. When passing through the water curtain, faster moving plates tend to incur less temperature drop than slower moving plates. This

is largely a result of less contact time between the water curtain and the heated surface at high plate velocities.

Further studies on the effect of motion on heat transfer during jet impingement boiling were undertaken by Chen et al. [10, 34-36] and Han et al. [8]. In their experimental work, an apparatus was developed to test the cooling conditions during impingement from a bottom jet. This essentially eliminates the effects of pooling as water from the jet will fall off the plate surface due to gravity. A notable observation in their studies was that the motion of the surface causes the shape of the water film to stretch along the moving direction. Thus, the jet leaves an elliptical footprint contrary to the circular one observed in stationary jet impingement experiments. They also found that surface motion does not affect the heat transfer conditions inside the impingement zone, and that the heat transfer coefficients reported are similar to ones observed in stationary experiments.

Prodanovic et al. [2, 37] performed moving plate experiments using a pilot-scale run-out table facility developed at the University of British Columbia. In these experiments, a single top jet nozzle was used and plate speed was set at 0.35 and 1.0 m/s, respectively. Aside from velocity, flow rate and liquid subcooling were also systematically varied. Their observations indicate that cooling rate increased with slower velocities as also observed by Hatta [33]. A plot of the calculated peak heat flux versus entry surface temperature is presented in Figure 2-12. The calculated peak heat flux is the maximum heat flux recorded as a result of the plate passing through the jet. The surface entry temperature is the surface temperature recorded prior to passing through the jet. Both values were calculated from subsurface temperature measurements

using inverse analytical methods. Prodanovic et al. also reported that the maximum heat flux occurred at surface temperatures between 300 and 350°C and that the size of the impingement zone increases with decreasing surface temperature.

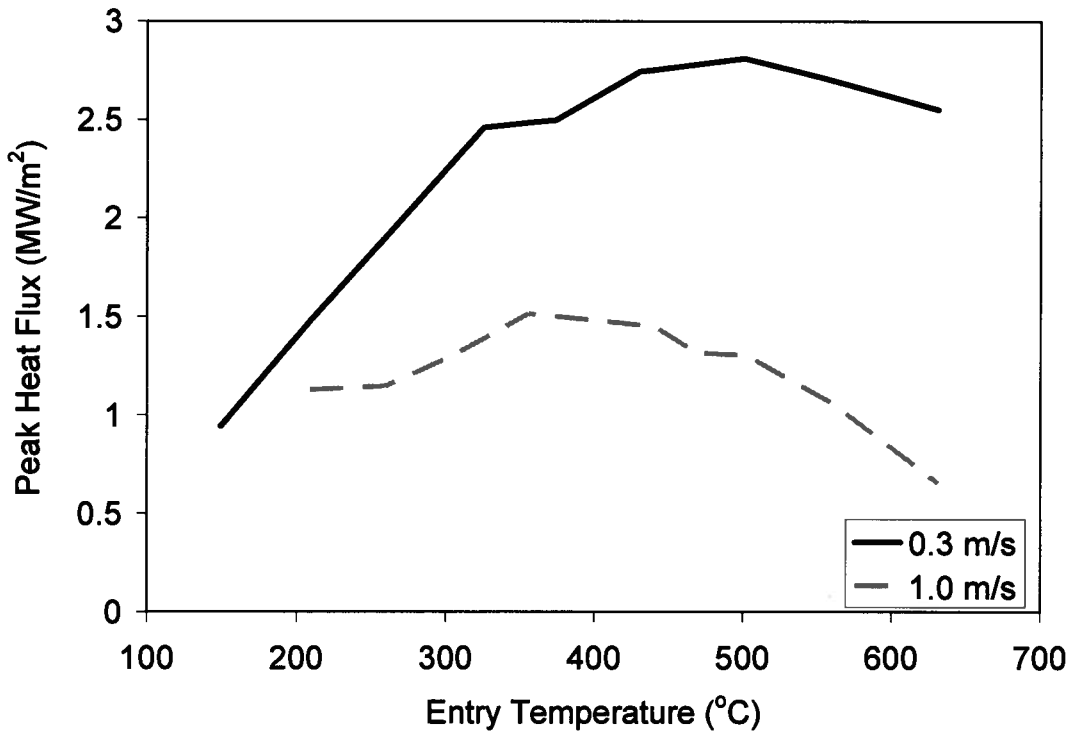

Figure 2-12 Peak surface heat flux as a function of entry temperature (modified from [37])

Johndale [38] followed up on investigations by Prodanovic et al. by incorporating three nozzles in one jet line in lieu of just one. Parameters investigated in his experimental work include water flow rate, plate speed and the spacing between nozzles. Johndale's results verified earlier observations that cooling rate increases with decreasing speed. However, the effect of plate speed on heat flux is not as significant in the nucleate boiling regime and its extent diminishes at lower entry temperatures. In addition, the results also indicated that the maximum heat flux recorded shifts to lower surface entry temperatures with increasing speed. Johndale also observed that much higher heat fluxes

were recorded inside the impingement zones than outside, which includes the interaction zones. With decreasing surface temperatures, the size of the impingement zones grow eventually encompassing the entire distance between nozzles. Heat flux across the impingement zones tend to be uniform, suggesting that uniform cooling can be attained if the impingement zones are deliberately allowed to converge with one another.

3. RESEARCH OBJECTIVES

The research objective of the present study is to investigate the effect of multiple water jet impingements on a moving hot steel plate. The experimental work serve as a follow up to initial moving experiments carried out by Johndale [38] and a second jet line of three nozzles is added to the investigation. In this particular study, the following parameters will be investigated

- jet line spacing
- jet line stagger
- plate speed

The aforementioned parameters are varied to investigate their effects on cooling efficiency. Cooling efficiency is characterized by the surface heat flux calculated from the temperature measurements. Special attention is placed on determining optimum jet configuration in both transverse and rolling directions that would allow maximum cooling efficiency while minimizing surface temperature gradients across the width of the plate. Results of this study will be used to improve understanding of jet interactions, which will lead to design optimization of industrial run-out table headers. The results will also form an experimental database for modeling of heat transfer and improving the hot mill model.

4. RESEARCH METHODS

4.1. Experimental Procedures

4.1.1. Test Facility

The UBC run-out table is a 20 m long pilot-scale facility that has been designed to simulate industrial cooling conditions that occur in hot strip mills. The facility has a moving test bed hence heat transfer studies on moving steel plates can be conducted. Thermal history of the test plate is recorded by installing sub-surface thermocouples on the test plate. A schematic of the facility and its main components are shown in Figure 4-1. A summary of the key specifications of the pilot-scale run-out table facility is presented in Table 4-1.

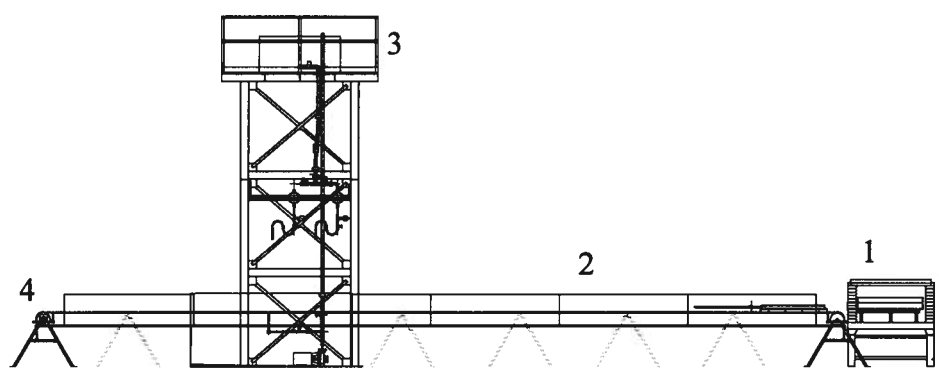

Figure 4-1 Schematic of pilot-scale run-out table at UBC

At one end of the facility is an electric furnace (1), where samples can be heated up to 1000 °C. The furnace is fitted with a gas line to supply nitrogen thereby providing an inert atmosphere that will minimize the formation of scale. Next to the furnace is a chain drive system (2) to transport the test sample for passes under the cooling section (3). The chain drive system measures 15 m in length with the initial 10 m situated prior

to the cooling section for acceleration of the test plates. At the other end of the chain drive is a hydraulic power unit (4) which drives a torqmotor to move the test plate through the cooling section at a prescribed speed. The motor can drive test plates up to a speed of 3.0 m/s. The speed of the chains is controlled by a computer generated voltage signal given to the proportional control valve on the hydraulic power unit.

The cooling tower measures 6.5 m in height and houses two tanks (top and bottom) as well as the headers and nozzles for top and bottom cooling systems. Both top and bottom cooling systems can be turned on concurrently. However, experiments only utilize either the top or bottom cooling system only as placement of thermocouples on the opposite surface provides only one available surface for investigation. A tank heater is situated in the upper tank and is primarily used for conditioning the water to the proper subcooling temperature. The bottom tank serves as a containment vessel for capturing water exiting the nozzles. A recirculation pump is used to recycle water back to the headers.

The top jet cooling system consists of two headers, each housing a jet line of three laminar jet nozzles. Flow to each header is controlled by electronic solenoid valves. Flow out of each nozzle is monitored with a turbine flow meter. The standoff distance between the plate and nozzle can be varied up to a maximum height of 1.5 m.

Signals from the thermocouples as well as measured flow rates from the flow meters are collected via two external data acquisition boards and transferred to a PC using DASYLab™ 7.0 data acquisition software. The software also manages outgoing voltages that control the hydraulic power unit.

Table 4-1 Summary of key specifications of pilot-scale run-out table

Electric heat furnace	Denver fire clay (208V, 92A, 60Hz) Maximum heating temperature:1000 °C
Water pump	15HP, 3600RPM, 60Hz
Upper tank	1.5×1.5×1.0m with 30kW heater
Lower tank	3×0.7×1.2m
Top Jet Lines	2
Top Nozzles	6
Bottom Nozzles	1

4.1.2. Material and Sample Preparation

The test samples used for this study are made from as-hot rolled high strength low alloy (HSLA) steel plates supplied by ArcelorMittal Dofasco located in Hamilton, Ontario. The plate dimensions are 1200 x 430 x 6.65 mm. The chemical composition of the steel is given in Table 4-2

Table 4-2 Steel sample chemistry

Element	Wt. %
C	0.0512
Mn	1.289
P	0.012
S	0.0041
Si	0.1015
Cr	0.0434
Ni	0.0127
Mo	0.0106
Al	0.0395
N	0.0045
Ti	0.0032
V	0.0061
Nb	0.0689
Fe	Balance

Each test plate is instrumented with eighteen 1.6mm type-K thermocouples, nine of which are primarily used for the analysis, and another nine serving as back-ups. The

thermocouples are stripped of their sheathing and embedded in 1.59 mm diameter holes drilled from the bottom of the plate to a depth of approximately 1 mm below the top surface. The thermocouple wires are spot welded to the bottom of the hole forming an intrinsic type thermocouple junction. Thermocouples along the lateral direction of the plate are placed 12.6 mm apart. The distance between the two sets of nine thermocouples is set at 25.4 cm or 50.8 cm depending on the jet line distance used for the experiment. A schematic of the plate and thermocouple locations for a jet line spacing of 25.4 cm is presented in Figure 4-3.

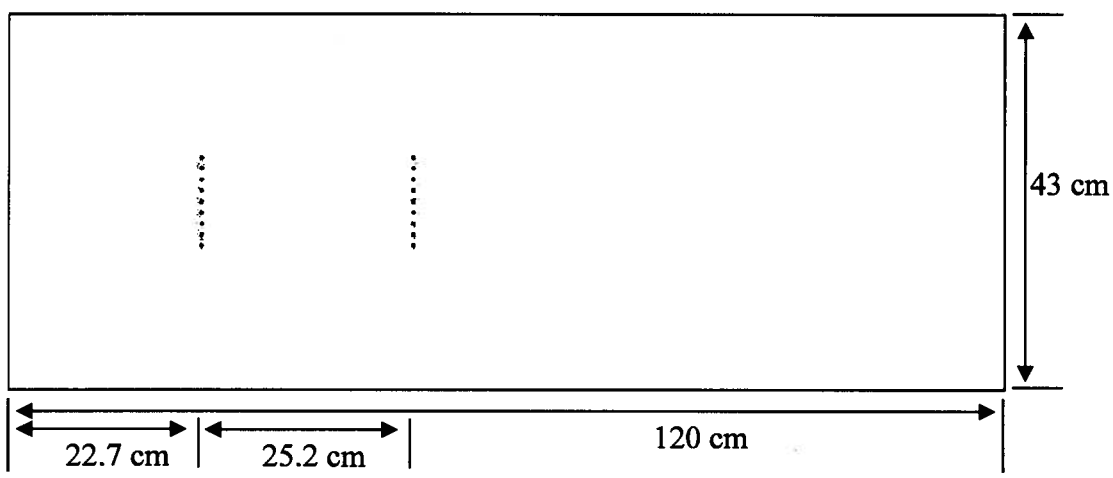

Figure 4-2 Schematic of sample test plate with dimensions and thermocouple locations

Prior to instrumentation, the test plate is first attached to a steel carrier. The carrier functions as a bed for the test plate so it can be placed and removed from the furnace and onto the chain drive system. After attachment to the carrier, the depth of the pre-drilled holes for the thermocouples is precisely measured. This is accomplished by inserting a probe of known length inside the hole. The portion of the probe that crops out of the hole is measured to determine the depth of the hole. The hole is subsequently

cleaned using methanol and pressurized air. Then, instrumentation with thermocouples can begin.

A schematic of the thermocouple installation is presented in Figure 4-3. Approximately 7mm of the original thermocouple sheathing is first removed to reveal the thermocouple wires. The wires are then inserted into a ceramic tube insulator. The ceramic tube ensures that the wires do not touch and temperature is measured at the intended location. The thermocouple wire and ceramic tube set-up is inserted into the pre-drilled holes located at the bottom of the test plate. The wires are then spot welded into the bottom of the hole. The sheathed portion of the thermocouples is anchored on the bottom surface of the test plate using screws to hold the thermocouple in place and to ensure that the wires remain welded in the hole.

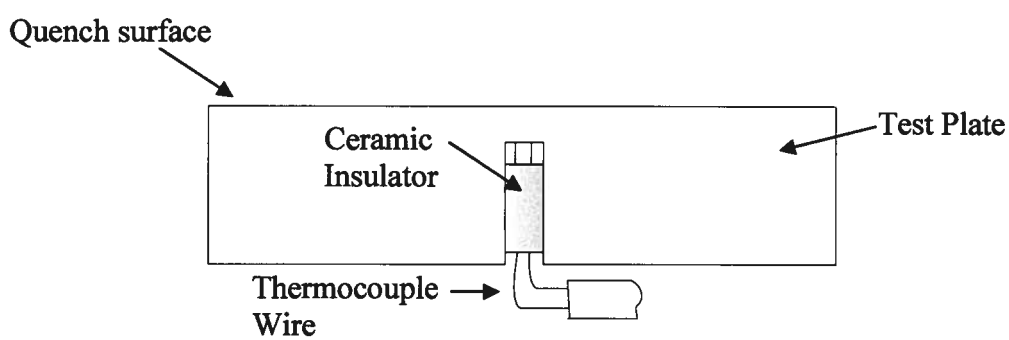

Figure 4-3 Cross-sectional view of thermocouple installation

4.1.3. Test Matrix and Procedure

A test matrix for this research has been devised to study the effect of jet line spacing, stagger and plate speed on heat transfer. Each jet line consists of three nozzles that are placed 1.5m above the moving steel plate. Jet line spacing is varied between 25.4 cm and 50.8 cm. Stagger is set at either 0 mm (no stagger), 25.4 mm or 50.8 mm.

Considering that the nozzle spacing is set at 100.8 mm, a 50.8 mm stagger will form an alternating array of nozzles between the first and second jet line. The plate speed is varied from 0.35 to 1.0 m/s. A total of 12 different set-ups are investigated. Details of the parameters for the tests presented here are summarized in Table 4-3. For all tests, a constant flow rate of 15 l/min is maintained for all nozzles and water temperature is held at 25 °C.

Table 4-3 Test Matrix

Set-up	Jet Line Spacing (cm)	Nozzle Stagger (mm)	Speed (m/s)
1	25.4	0	0.35
2	25.4	0	1.0
3	25.4	25.4	0.35
4	25.4	25.4	1.0
5	25.4	50.8	0.35
6	25.4	50.8	1.0
7	50.8	0	0.35
8	50.8	0	1.0
9	50.8	25.4	0.35
10	50.8	25.4	1.0
11	50.8	50.8	0.35
12	50.8	50.8	1.0

Considering the thermocouple configuration presented in Figure 4-3, the nozzles are arranged in such a way that temperature measurements in both the impingement and interaction zones are taken, regardless of the nozzle configuration (stagger) deployed. Close-up views of the thermocouple configuration with the expected impingement zones of each stagger configuration are presented in Figure 4-4, Figure 4-5 and Figure 4-6. As can be seen from the figures, the 2 groups of 9 thermocouples capture information on a 100.8 mm band of the plate. In the non-staggered case (Figure 4-4), the centre nozzles of each jet line pass through the centre-line of the 100.8 mm measurement band. To form

the staggered arrangements, both jetlines are adjusted by moving both about the centre-line in opposite directions.

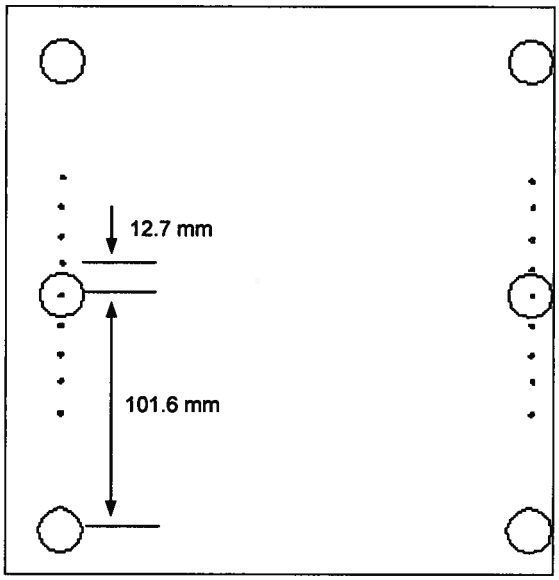

Figure 4-4 TC configuration and expected impingement from no stagger case

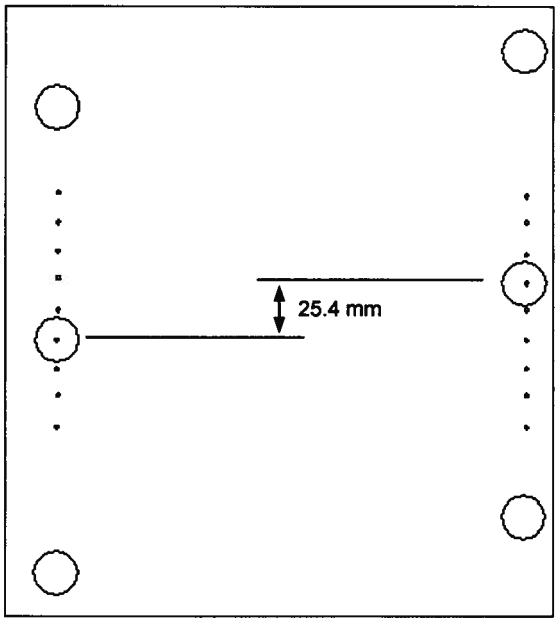

Figure 4-5 TC configuration and expected impingement from 25.4 mm stagger case

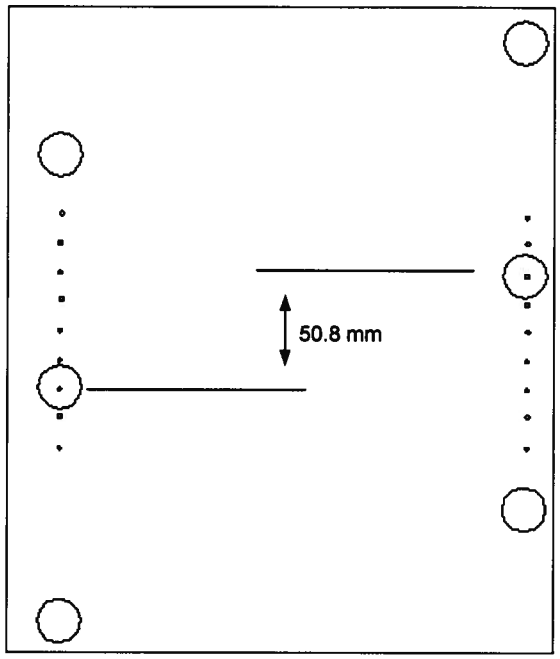

Figure 4-6 TC configuration and expected impingement from 50.8 mm stagger case

After instrumenting the plate, the plate-carrier assembly is placed on the chain drive system. The location of the thermocouple holes are marked on the top surface of the test plate using permanent ink. The plate-carrier assembly is then positioned underneath the nozzles and the circulation pump is turned on to allow water flow through the nozzles. The nozzles are adjusted such that impingement occurred at the marked locations as presented in Figure 4-4. After adjustment of the nozzles, the thermocouples are connected to the data acquisition system and the plate-carrier system is placed in the furnace.

While the test plate is in the furnace, water from the bottom tank is pumped to the top tank for temperature conditioning. The water temperature is set and maintained at 25 °C for all the tests. Upon reaching the set temperature, the top tank is emptied into the

bottom tank. Water temperature is maintained through controlled adjustments by addition of hot (~50 °C) or cold (~15 °C) tap water.

In the experiments, the plate is heated to 850 °C in order to attain a first pass under the cooling section at approximately 700 °C. After the pass, flow from the nozzles is temporarily stopped, and the plate is moved back and allowed to thermally equilibrate. The plate is then moved through the cooling section to simulate a next pass at lower temperatures. The process is repeated until the plate temperature no longer rebounds above 150 °C.

4.2. Analytical Procedures

4.2.1. Inverse Heat Conduction Analysis

Sub-surface temperature measurements during run-out table cooling experiments are useful data in studying the heat transfer processes that take place. However, inverse heat conduction (IHC) algorithms provide a means of using the measured temperature history to calculate the heat flux and temperature history at the quench surface. In the present study, all temperature-time data were analyzed using the IHC model developed by Zhang [39].

This IHC model utilizes finite element and inverse methods to predict the heat-transfer boundary condition at a surface by using the thermal history at a known interior location. Calculation of the surface heat flux and temperature is accomplished through a two-step process. First, an initial guess for heat flux is used and the direct solution to the heat conduction problem is determined by calculating the temperature evolution after a predetermined number of future time steps. In the second step, the inverse routine

compares the measured temperature values with the calculated temperature values. The difference between the measured and calculated values is then used to calculate a new heat flux and the first step is repeated. This process continues until a set of pre-determined convergence criteria have been met. Details of the convergence criteria and other aspects of the IHC model used are given in Reference 39.

The IHC model considered a 2-D axisymmetric domain representing both the sample and the thermocouple as shown in Figure 4-7. TR and TD denote the thermocouple radius and depth, respectively. For all IHC analyses in this study, TR is constant at 0.8 mm. The domain is meshed using linear elements. A finer mesh is applied in the areas adjacent to the quench surface as larger gradients are expected in this region. Details of the mesh density and element size at the various areas of the domain are presented in Table 4-4. It should be noted that the values summarized in Table 4-4 are for the condition where TD is 1 mm. For each calculation, the domain used is updated and adjusted such that the precise measured dimension for TD is used.

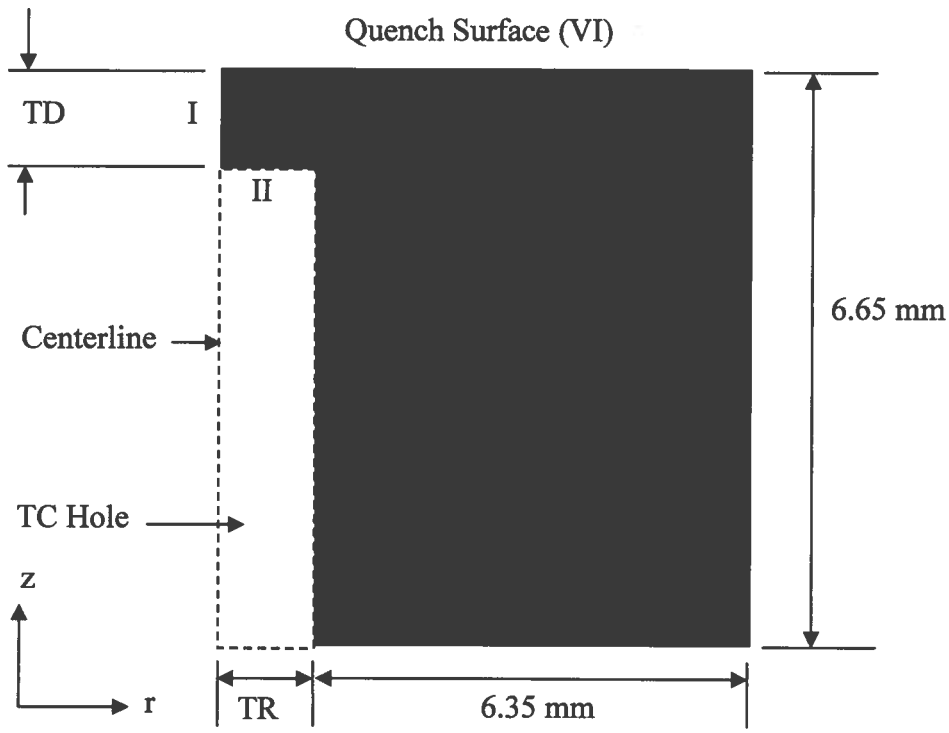

Figure 4-7 2-D axisymmetric domain used in IHC analyses

Table 4-4 Mesh density information and size of elements

Section	Elements	Arrangement (r × z)	Element Size (mm)
A	25	5 × 5	0.16 × 0.21
B	50	10 × 5	0.555 × 0.210
C	100	10 × 10	0.555 × 0.560

The model also requires the thermophysical properties of the material that is investigated. There is no available specific data for the HSLA steel used in the experiments. Instead, values taken from literature for steel with similar chemistry – AISI 1008 – are used in this study [40]. A summary of these properties is presented in Table 4-5.

Table 4-5 Material properties of steel used in IHC model

Property	Value
Conductivity: k	60.571–0.03849×T [W/m°C]
Density: ρ	7800 [kg / m^3]
Specific heat: c_p	470 [J / kg °C]

It is imperative to include the thermocouple in the analysis because under high surface heat flux conditions, the presence of the thermocouple creates errors in the calculation of heat flux at the surface [41]. This is attributed to the presence of the thermocouple hole, which has a much lower thermal conductivity than the steel sample. Since the thermal conductivity of the thermocouple hole is much less than that of the steel, heat transfer through the thermocouple-sample boundaries becomes negligible and an adiabatic hole can be used in lieu of the actual thermocouple [42].

The use of a 2-D axisymmetric domain is an approximation of the actual situation being considered. When the plate passes through the cooling section, the impingement zone travels from one end of the plate to the other and passes directly on top of certain thermocouples only. Hence, the cooling response surrounding each thermocouple is not truly axisymmetric as the cooling conditions would also induce gradients in the θ–direction. This would necessitate use of more complex 3-D analyses instead. However, previous study by Chan [43] showed that these gradients are an order of magnitude less than the gradients experienced in the z-direction and can be considered negligible. Thus, using a 2-D axisymmetric domain as a simplification to the problem is valid. The also model makes another simplification by not accounting for the latent heat generated during phase transformation.

The finite element portion of the IHC model directly solves the heat conduction equation as presented by

$$\frac{1}{r}\frac{\partial}{\partial r}\left(kr\frac{\partial T}{\partial r}\right)+\frac{\partial}{\partial z}\left(k\frac{\partial T}{\partial z}\right)=C_{\rho}\frac{\partial T}{\partial t} \qquad 4\text{-}1$$

where k is the thermal conductivity (W/m·K), C_p is the volumetric specific heat (J/m^3) and t is the time (sec). Referring to Figure 4-7, the applicable boundary conditions for the model are defined as follows:

I. Due to symmetry, there is no heat flow across the centreline

$$-k\frac{\partial T}{\partial r}\bigg|_{r=0}=0 \qquad 4\text{-}2$$

II. An adiabatic condition is assumed between the thermocouple and the sample, i.e. there is no heat flow between the thermocouple and the sample

$$-k\frac{\partial T}{\partial z}\bigg|_{0<r<TR,z=(z_{max}-TD)}=0 \qquad 4\text{-}3$$

III. As with boundary II, an adiabatic condition is assumed between the thermocouple and the sample.

$$-k\frac{\partial T}{\partial r}\bigg|_{r=TR,0<z<(z_{max}-TD)}=0 \qquad 4\text{-}4$$

IV. Heat flow through the bottom boundary is governed by both convection and radiation. However, heat transfer by radiation is much larger than convection at high temperatures. Hence, contributions from convective heat transfer are deemed negligible and ignored in the model. The underlying boundary condition is governed by:

$$h_r=\sigma\varepsilon\left(T^2+T_{\infty}^2\right)\left(T+T_{\infty}\right) \qquad 4\text{-}5$$

where σ is the Stefan-Boltzman constant, ε is the emissivity and T_∞ is the ambient temperature. Emissivity is a function of temperature in °C such that

$$\varepsilon = \frac{T}{1000}\left(0.125\frac{T}{1000} - 0.38\right) + 1.1 \qquad \text{4-6}$$

V. The boundary away from the TC hole forms the border between steel that is inside and outside of the domain. A semi-infinite solid is assumed such that thermal conduction is present as shown by

$$q\big|_{r=r_{\max}} = -k\frac{\partial T}{\partial r}\bigg|_{r=r_{\max}} \qquad \text{4-7}$$

VI. The quenched surface is the unknown boundary being calculated by the IHC model. During running of the finite element portion of the model, this boundary corresponds to an applied surface heat flux q.

$$q = -k\frac{\partial T}{\partial z}\bigg|_{z=z_{\max}} \qquad \text{4-8}$$

The starting temperature measured by the thermocouple also serves as the initial condition of the model. It is assumed that at the beginning of a test, a uniform temperature exists throughout the domain.

$$T(r,z)\big|_{t=0} = T_i \qquad \text{4-9}$$

4.2.2. Interpolation of Measured Temperature Data

One of the limitations of IHC algorithms is their dependence on data frequency to calculate highly dynamic heat flux conditions. Such can be the case in run-out table cooling experiments as abrupt changes in heat flux are expected when the plate moves in and out of the water jets. This difficulty arises from the manner in which the inverse portion of the IHC model calculates the heat flux. Surface heat flux is calculated by determining the required change in heat flux necessary to induce the measured temperature change from the current time position being evaluated to a predetermined future time step. This calculated rate of change in heat flux is then used to calculate the heat flux in the next time increment.

When the data frequency is low, there may be insufficient data points surrounding abrupt changes in temperature, inhibiting convergency between the solution and the measured temperature. An example of this IHC limitation is presented in Figure 4-8. The figure shows a typical measured temperature history recorded during a pass under one jet at 1 m/s and the predicted temperature history calculated by an IHC model. In this case, data was acquired at the maximum rate of 30 Hz. The figure also shows that the solution does not converge with the initial temperature measurement. There are not enough data points during the temperature drop to establish the proper slope that is actually experienced in this region. Because a much less pronounced temperature drop is calculated by the IHC model, the corresponding calculated heat flux is also expected to be less.

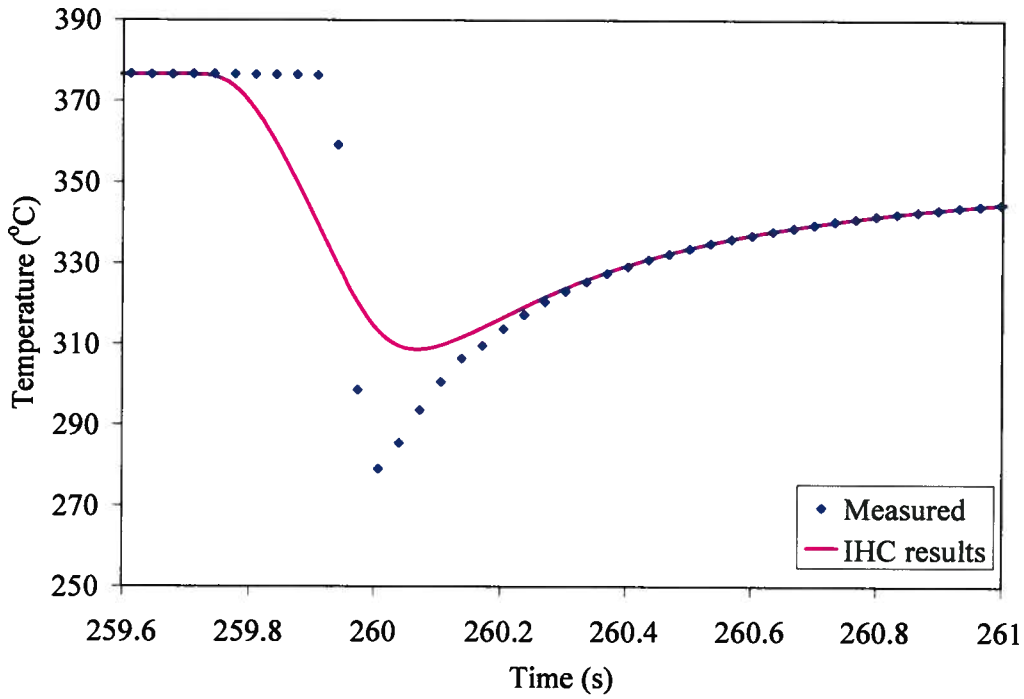

Figure 4-8 Comparison of measured temperature and IHC results

To ensure that the measured temperature history converges with the solution, it is imperative that the data set being analyzed has sufficient data frequency. This can be accomplished by using higher data acquisition rates or introducing data points in between existing ones through interpolation. With more data points, the IHC calculations are allowed to "catch up" and settle into the proper slope prior to another abrupt change. The effect of using higher data frequencies is presented in Figure 4-9. The original measured temperature curve is reproduced by linearly interpolating a data point between existing ones, thus doubling the effective data frequency. As seen on the figure, the IHC predicted values converged better with the measured values. Its effect on the subsequent surface heat flux calculation is also shown in Figure 4-10.

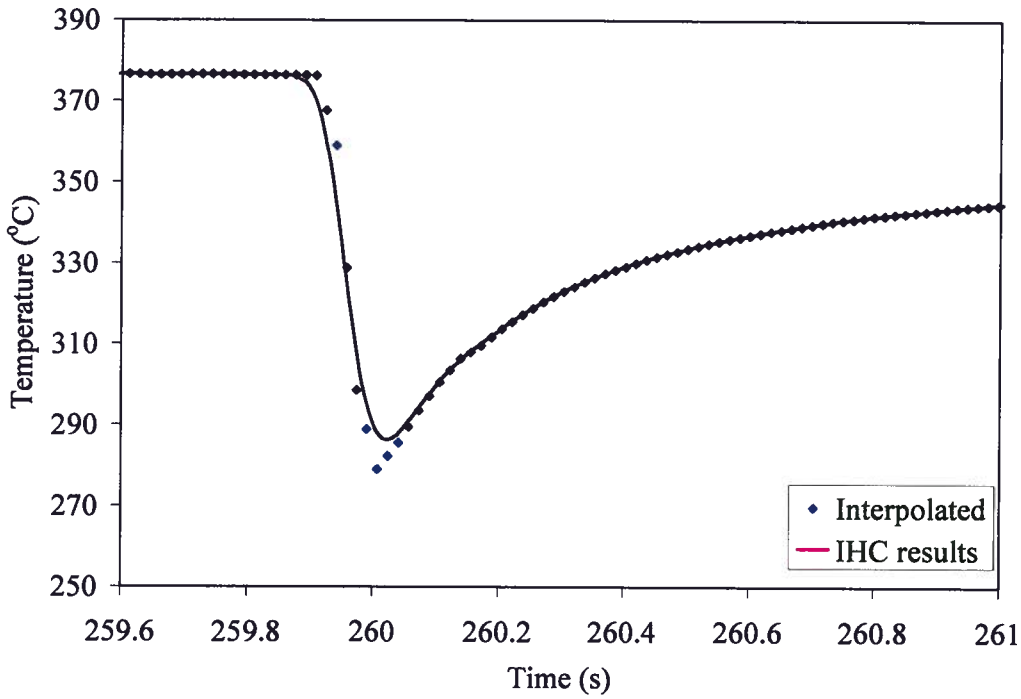

Figure 4-9 Comparison of interpolated measured temperature and IHC results

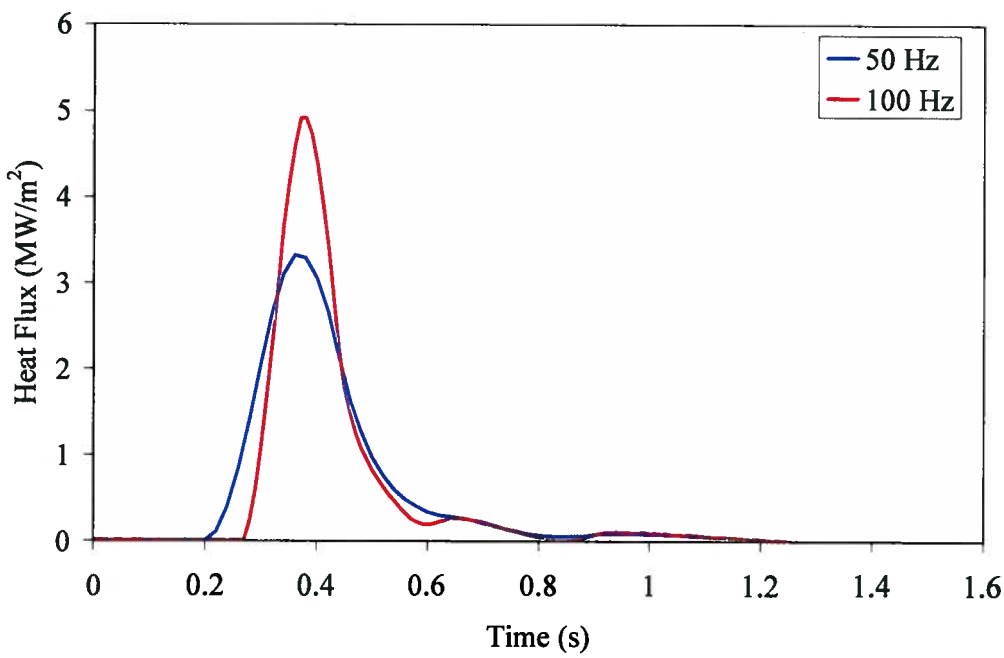

Figure 4-10 Comparison of heat flux values calculated by IHC analysis with different acquisition rates

In the experiments, the maximum data acquisition rate that can be attained is governed by the number of thermocouples used in the study. In the present set-up of 18 thermocouples, the maximum acquisition rate obtained is 50 Hz. This low acquisition rate does not constitute the measured data as unsuitable for analysis using the IHC model. It is worth noting that very little noise is observed in the measured data, as exemplified by the smooth trend in Figure 4-8. This allows the use of spline routines to create additional data points. The smoothness of the measured values suggests that interpolated points in between the existing data set are valid assumptions of the overall temperature history. Thus, to further improve the data frequency, the measured temperature history data is subjected to spline interpolation. A routine is developed using Sigmaplot™ software to produce an interpolated data point in between existing data points, thus effectively doubling the data frequency to 100 Hz. A first order spline or linear interpolation was used.

5. RESULTS AND DISCUSSION

5.1. Temperature Curves

Representative cooling curves of measured sub-surface temperature versus time are presented in Figure 5-1. The data shown in Figure 4 are from the test performed without stagger, jet line spacing of 25.4 cm and plate speed of 1.0 m/s (Set-up 1). Temperature readings are from the central thermocouple which passes directly under the stagnation zone of both centre nozzles, as depicted in Figure 4-4.

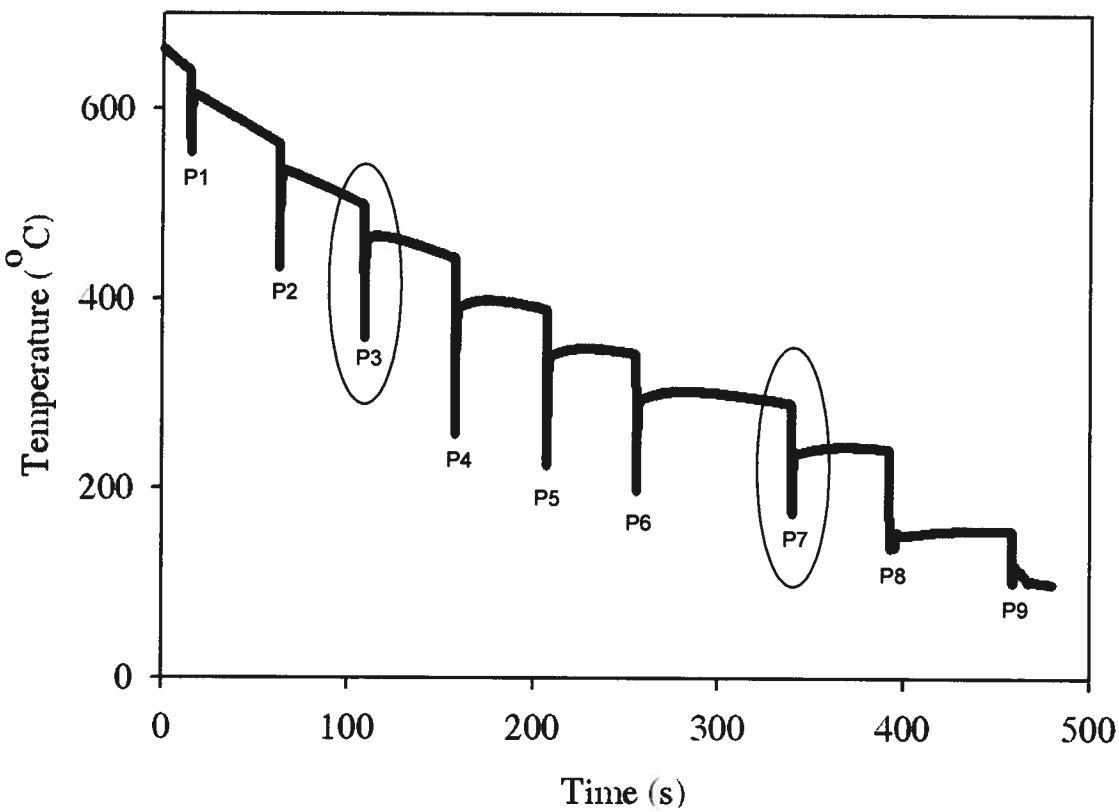

Figure 5-1 Measured thermal history for Test 2 (speed = 1 m/s, spacing = 25.4 cm, stagger = 0 mm)

Figure 5-1 shows a clear trend of the thermal history observed during a test. When the plate passes through the cooling section, an immediate decrease in temperature is experienced and is indicated as P1, P2 etc. After the plate leaves the cooling section,

the temperature of the steel begins to rebound due to the thermal mass of the plate. A closer look at individual passes is presented in Figure 5-2 and Figure 5-3, respectively, wherein the time scale is reset to zero when the front edge of the plate reaches the first jet line. Figure 5-2 shows the temperature evolution during the pass initiated at 500 °C (P3) and Figure 5-3 depicts the pass initiated at just below 300 °C (P7).

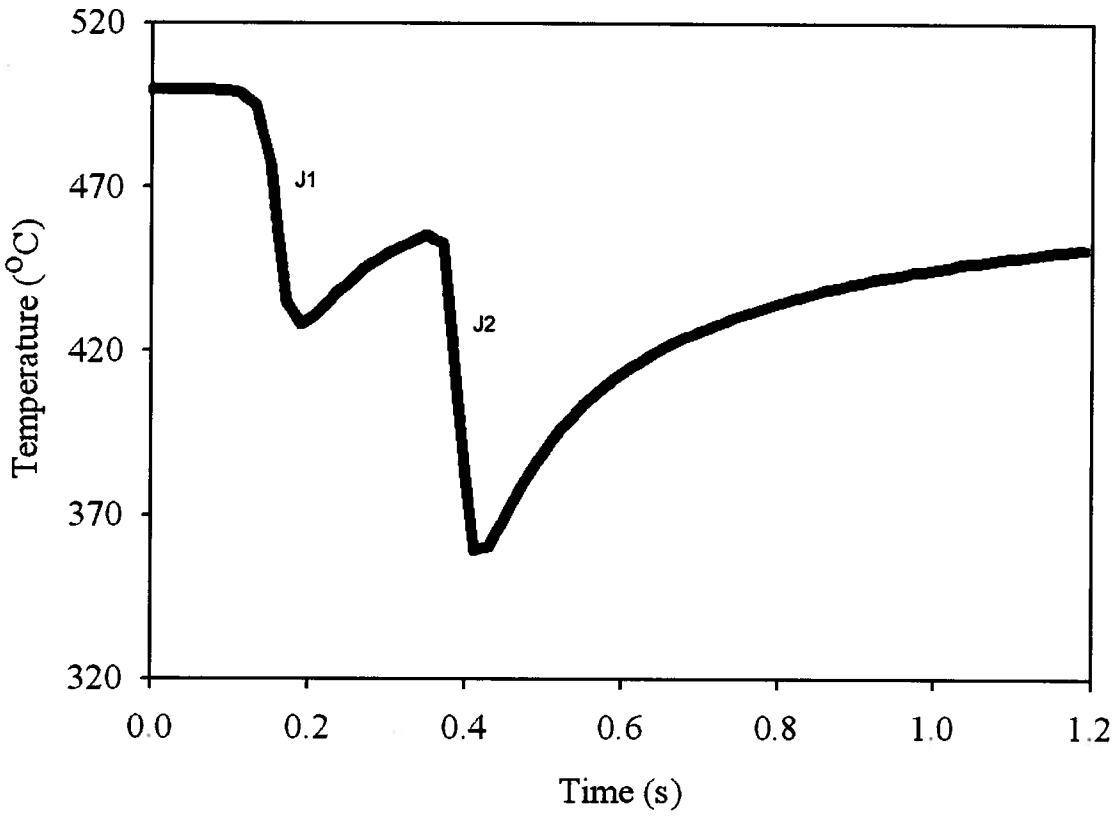

Figure 5-2 Close-up of measured thermal history with starting temperature of 500 °C (Pass 3, Test 2)

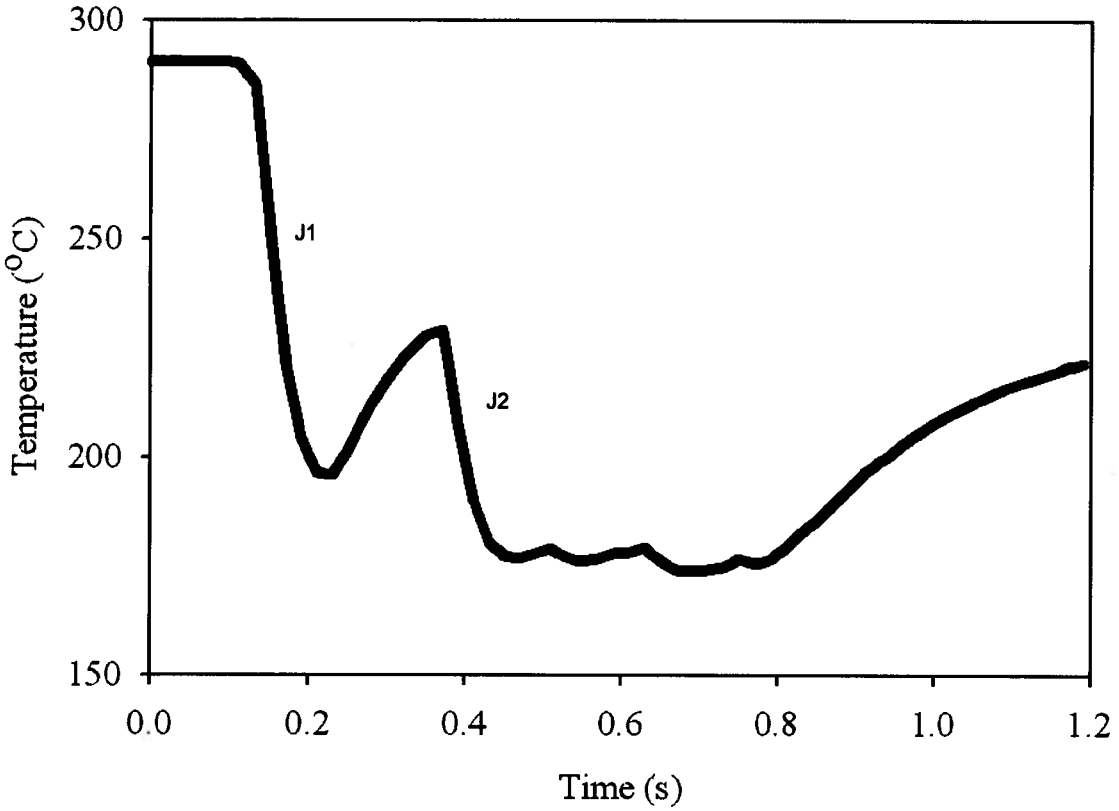

Figure 5-3 Close-up of measured thermal history with starting temperature of 300 °C (Pass 7, Test 2)

Figure 5-2 and Figure 5-3 reveal that the cooling of each jet line (J1 and J2) can be discriminated from one another. In between jet lines, the temperature of the steel rebounds partially in a similar manner as in between passes. This is indicative that water evaporates in between jet lines at these temperatures. From Figure 5-2, it can be discerned that a larger drop in temperature is observed from the second line, suggesting a higher heat flux than under the first line. The opposite is observed at lower temperatures as depicted in Figure 5-3. Further, the rate of evaporation considerably decreases at lower temperature and pooling of water can be observed after the pass as evidenced by the delayed onset for the steel temperature to rebound (Figure 5-3).

5.2. Heat Flux Curves

The calculated surface heat flux history corresponding to the measured temperature history in Figure 5-1 is presented in Figure 5-4.

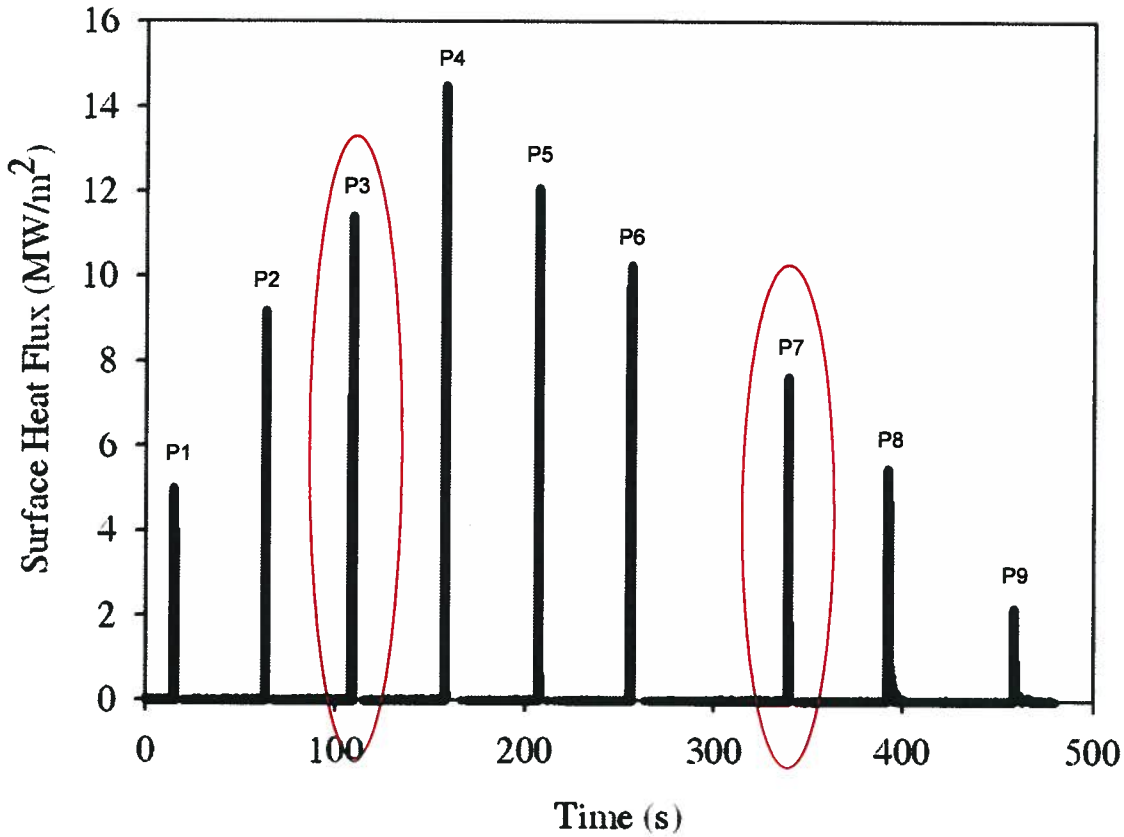

Figure 5-4 Calculate surface heat flux history for Test 2 (speed = 1 m/s, spacing = 25.4 cm, stagger = 0 mm)

Similar to the measured temperature history, the individual passes can be easily demarcated in the plot. When the plate passes through the jets, spikes in the heat flux curve are observed. The overall trend of the plot suggests that as the water impinges on the surface, cooling immediately begins and the heat flux suddenly increases to a maximum or peak value. After the plate leaves the jet, cooling halts and very little to no heat flux is recorded in the regime of air cooling. A closer look at individual passes is

presented in Figure 5-5 and Figure 5-6, respectively. These figures correspond to the measured temperatures presented in Figure 5-2 and Figure 5-3, respectively, with plate temperatures of 500 °C and 300 °C, respectively.

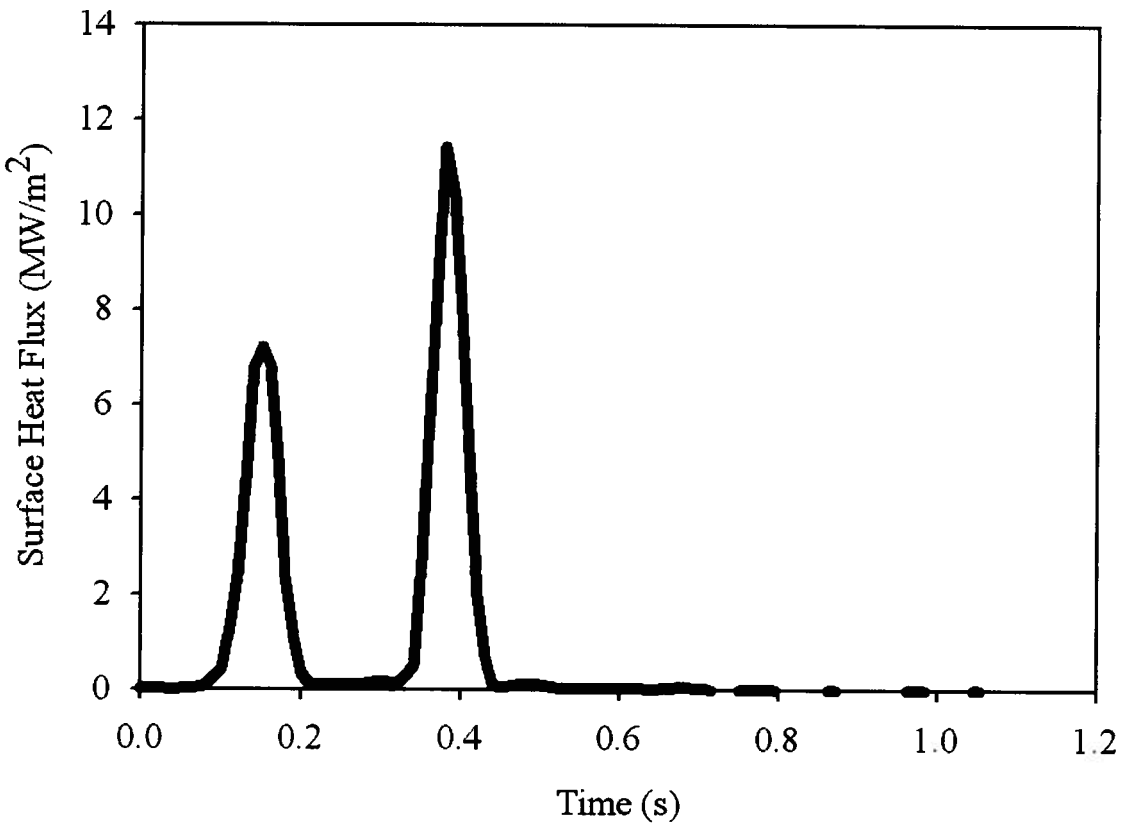

Figure 5-5 Close-up of the calculated heat flux history with starting temperature of 500 °C (Pass 3, Test 2)

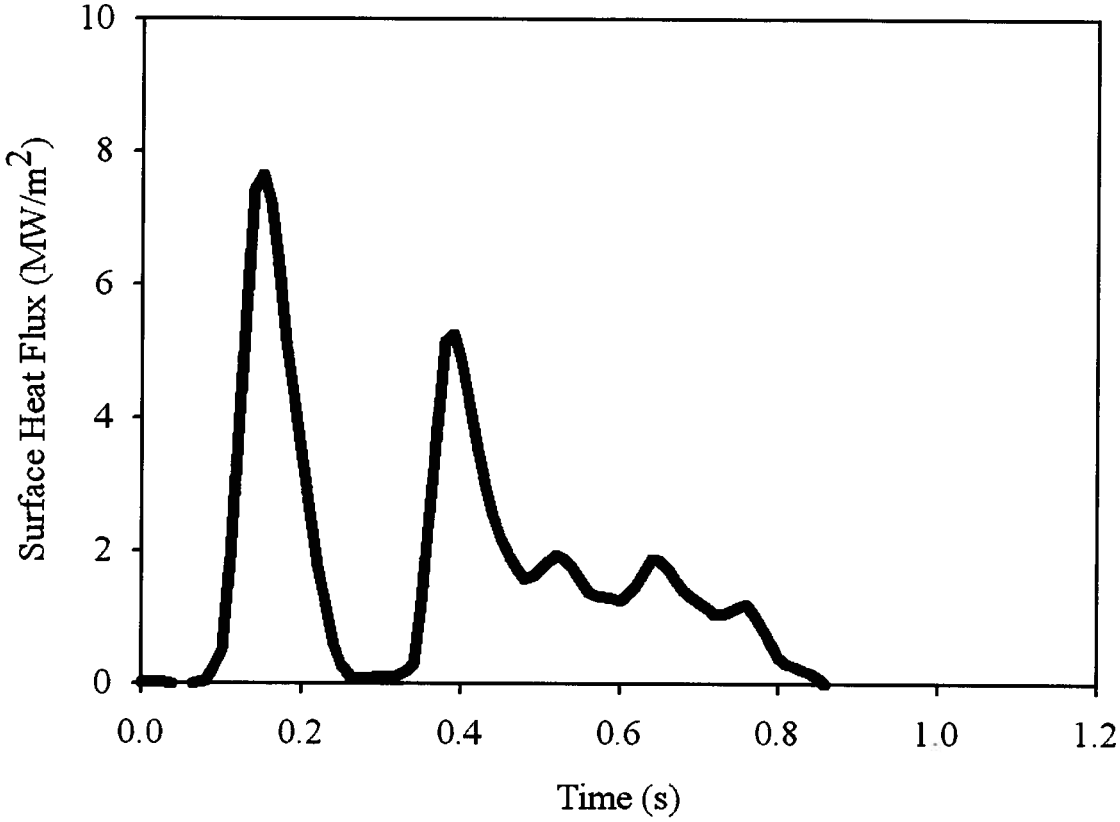

Figure 5-6 Close-up of the calculated heat flux history with starting temperature of 300 °C (Pass 7, Test 2)

Figure 5-5 and Figure 5-6 verify initial observations using the thermal histories presented in Figure 5-2 and Figure 5-3. During a pass initiated at a higher temperature, as in the case of Figure 5-5, the peak heat fluxes attained under the impingement zone appear to increase with decreasing temperature. This is indicative that at these temperatures, transition boiling is experienced under the impingement zone. The absence of any elevated heat flux in between jet lines suggests that water completely evaporates in between the jet lines. At lower temperatures, as in Figure 5-6, the peak heat fluxes tend to decrease with temperature. This suggests that at these temperatures nucleate boiling is

experienced under the impingement zone. It can also be observed that after passing through the second jet line, a "tail" is formed suggesting elevated heat fluxes beyond the impingement zone. This indicates that water pools and contributes to the heat extraction after leaving the second jet line, until the water completely evaporates.

To further examine the trends presented in Figure 5-5 and Figure 5-6, the peak heat fluxes are plotted and shown in Figure 5-7 for all passes as a function of the surface entry temperature prior to each jet line. The heat fluxes follow a similar trend with temperature than that of a typical boiling curve. A maximum peak heat flux is observed in the range of 350 to 400 °C. At higher surface entry temperatures, heat flux increases with decreasing temperature, which is consistent with transition boiling and depicts the situation shown in Figure 5-5. At lower surface entry temperatures, heat flux decreases with decreasing temperature, and this is synonymous with nucleate boiling as reflected in Figure 5-6.

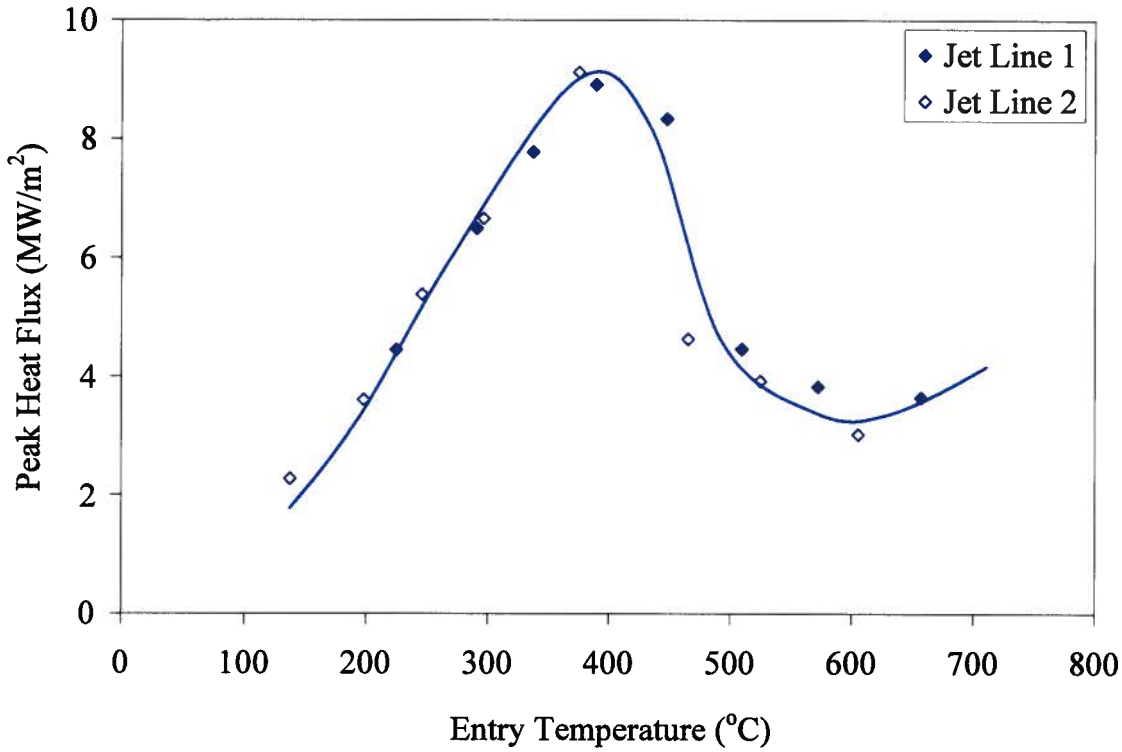

Figure 5-7 Plot of peak heat fluxes with respect to surface entry temperature for Test 2 (speed = 1 m/s, spacing = 25.4 cm, stagger = 0 mm)

5.3. Surface Contour Plots

Analysis of the IHC result from each individual thermocouple provides valuable insight into the different cooling conditions experienced at different areas of the plate with respect to the location of the impingement zones. In order to gain a better appreciation of the overall cooling conditions for the different nozzle configurations tested, the results at each thermocouple location are combined to construct contour plots. The contour plots are obtained by translating the surface heat flux and temperature data from varying in time to varying spatially based on the plate speed. These contour plots depict the surface temperatures and heat fluxes over the areas including and surrounding the impingement zones. An example of these is presented in Figure 5-8 and Figure 5-9 for surface heat flux and temperature, respectively with test conditions of 1 m/s, 25.4 cm

jet line spacing and no nozzle stagger. The moving direction is from left to right and the entry temperature is 500 °C. Significant gradients of surface temperatures and heat fluxes are recorded in this case without stagger when considering positions that fall in to the jet impingement zone versus positions in between jet impingement.

As with observations made in Chapters 5.1 and 5.2, the cooling effects as depicted by the surface heat flux and temperature show a dependence on the entry temperature, particularly in the region directly underneath the nozzles. Since the surface temperature is lower after passing through the first jet line, the subsequent heat fluxes recorded through the second jet line are much larger, following the trend presented in Figure 5-7. In the interaction zones, very little to no heat flux is recorded, indicating that the film boiling regime persists in these areas.

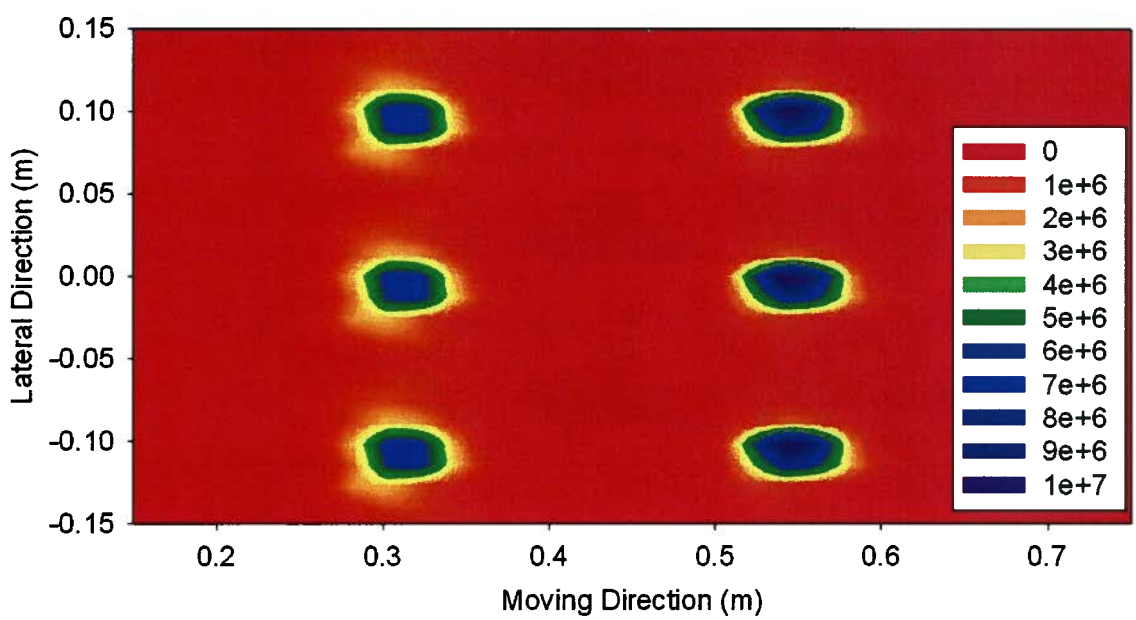

Figure 5-8 Contour plot showing the surface heat flux (W/m^2) for the test with no stagger and an entry temperature of 500 °C

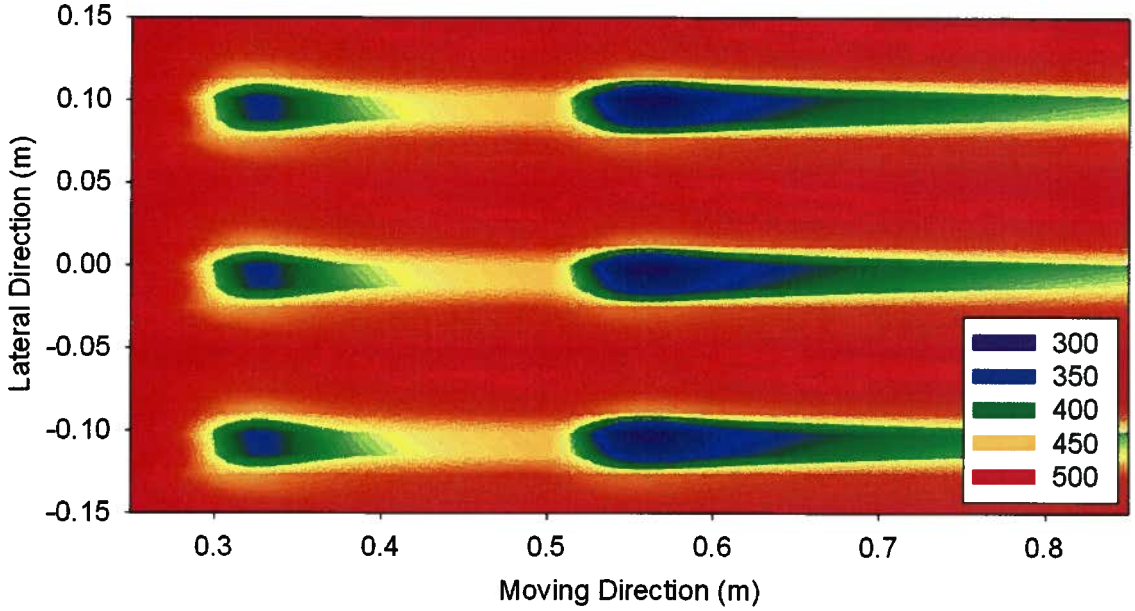

Figure 5-9 Contour plot showing the corresponding surface temperatures (°C) for the test with no stagger and an entry temperature of 500 °C

A comparison of the surface heat fluxes of two different nozzle configurations, i.e. without and with full (50.8 mm) stagger, is presented in Figure 5-10 and Figure 5-11, respectively. For both cases, the jet line spacing is maintained at 25.4 cm, plate speed was set at 1 m/s, and the passes are initiated at a temperature of 350 °C. Figure 5-10 represent the results without any stagger, while Figure 5-11 shows the situation for a stagger of 50.8 mm.

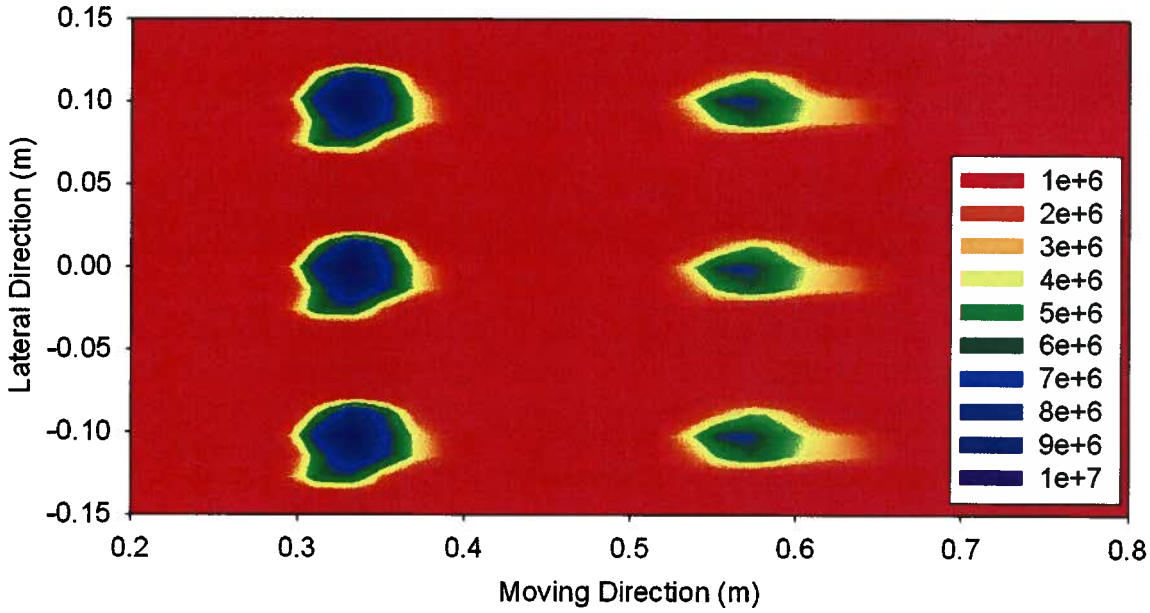

Figure 5-10 Contour plot showing surface heat flux (W/m^2) in a non-staggered configuration with an entry temperature of 350 °C

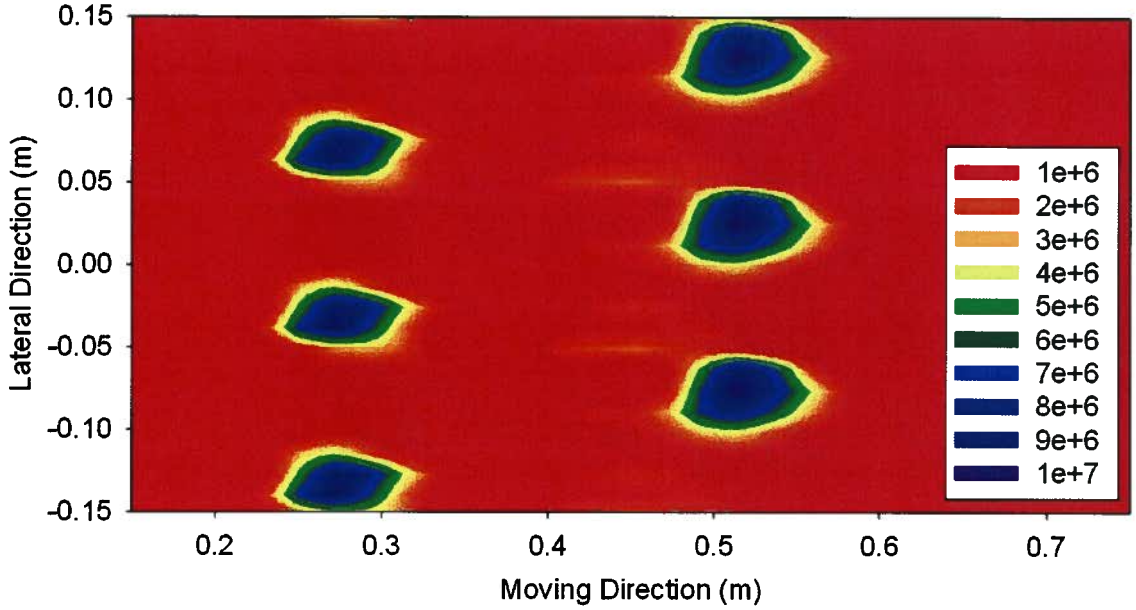

Figure 5-11 Contour plot showing surface heat flux (W/m^2) in a staggered nozzle configuration with an entry temperature of 350 °C

It can be discerned from Figure 5-10 that in the case without stagger, there is clearly a difference in the set of peak heat fluxes observed under the two jet lines. As with Figure 5-8, this follows the trend previously presented in Figure 5-7, i.e. higher heat fluxes in the first jet line. Very little to no heat flux is recorded in the interaction zones in between nozzles within the same line. However, for the staggered nozzle configuration, similar heat fluxes are observed under both the first and the second jet line. For the staggered case, minimal cooling occurs in the interaction zones of the first jet line. Hence, by the time these areas are about to be impinged by the second jet line, the surface temperature at these areas have changed very little. Since the areas impinged by the second jet line are at or near the temperature of the areas impinged by the first line, similar heat fluxes are recorded from the two jet lines.

Figure 5-12 and Figure 5-13 present the contour plots of the surface temperatures for the test conditions shown in Figure 5-10 and Figure 5-11. It can be seen from Figure 5-12 that with no stagger the same areas are being impinged and the entry temperature prior to each jet line is progressively lower. The heat extraction during the subsequent impingement reflects this change in surface temperature. In between nozzles, the temperature remains relatively unchanged. However, from Figure 5-13, it can be discerned that in the case of stagger, the areas impinged by the second jet line have similar entry temperatures as the areas impinged by the first line. As a result, similar heat extraction is observed from both sets of jet impingements, consistent with the results shown in Figure 5-11.

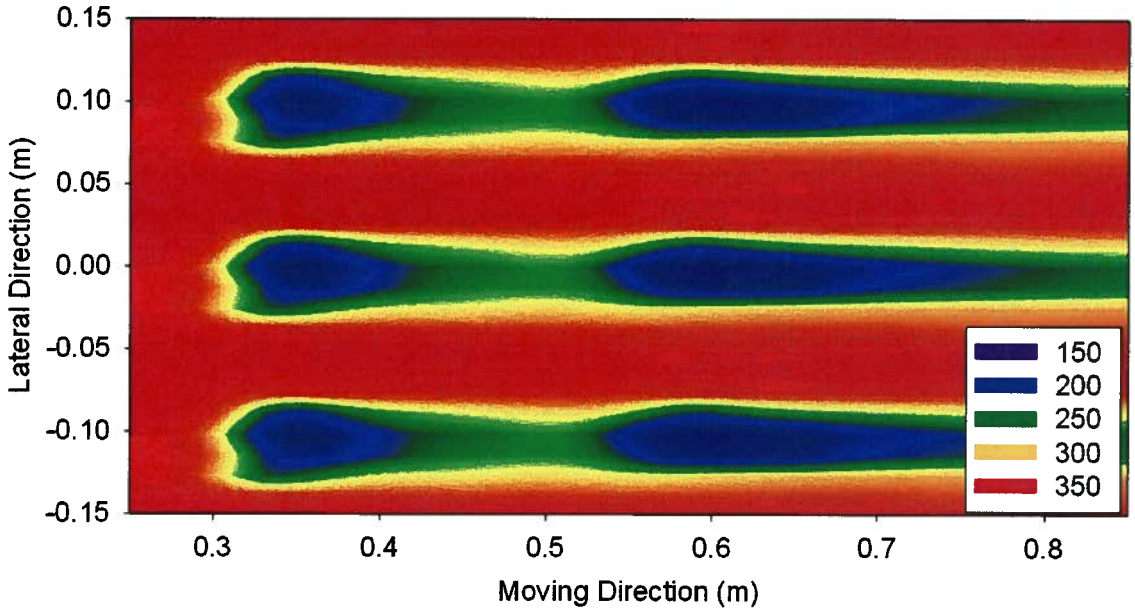

Figure 5-12 Contour plot showing surface temperature (°C) in a non-staggered nozzle configuration with an entry temperature of 350 °C

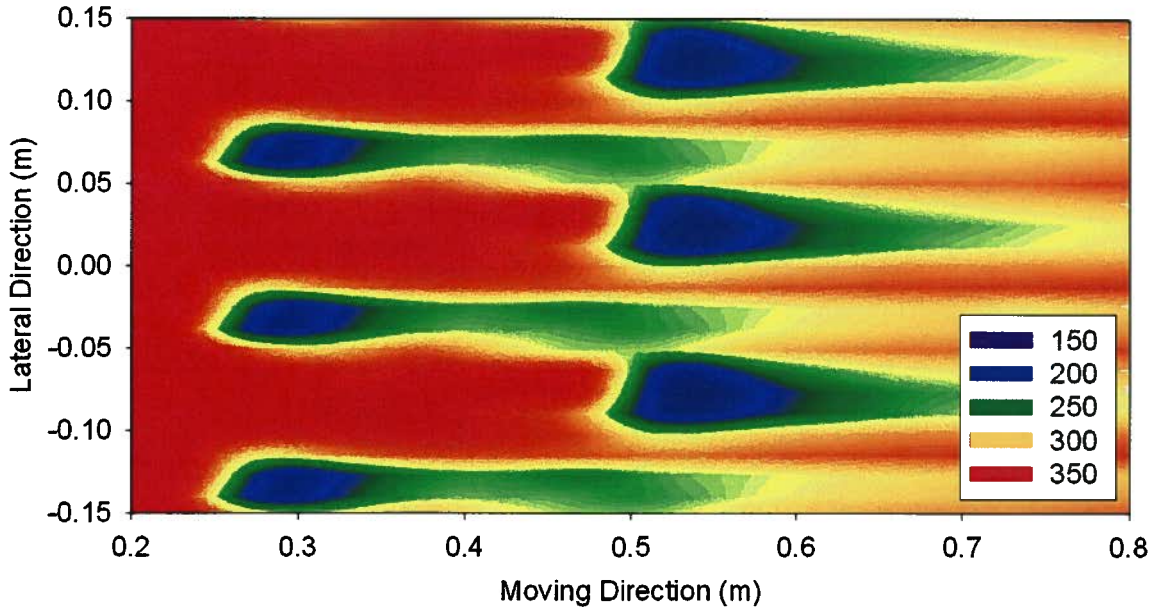

Figure 5-13 Contour plot showing surface temperature (°C) in a staggered nozzle configuration with an entry temperature of 350 °C

In the median case where stagger is set at 25.4 mm, the results depict a mix of the observations taken from the case without and with full stagger. The surface heat flux and temperature contour plots for the same plate speed, jet line spacing and entry temperature are presented in Figure 5-14 and Figure 5-15, respectively.

From the figures above, it can be concluded that impingement zones of the second jet line is larger than the impingement zones of the first jet line. This observation is particularly more evident in the surface temperature contour plot (Figure 5-15). This is believed to be due to the colder surface temperature in the wake of the first jet line. Since the impingement zone of the second jet line overlaps this colder zone, the water is able to readily wet this area as well, producing an enlarged foot print. Since there are different entry temperatures, the heat fluxes observed are also different and correspond to its respective entry temperature. Looking at the impingement zones of the second jet line, the area in the wake of the first jet line recorded lower heat fluxes. In the areas of the impingement zones not previously impinged, the heat fluxes observed are the same magnitude as those in the impingement zones of the first jet line.

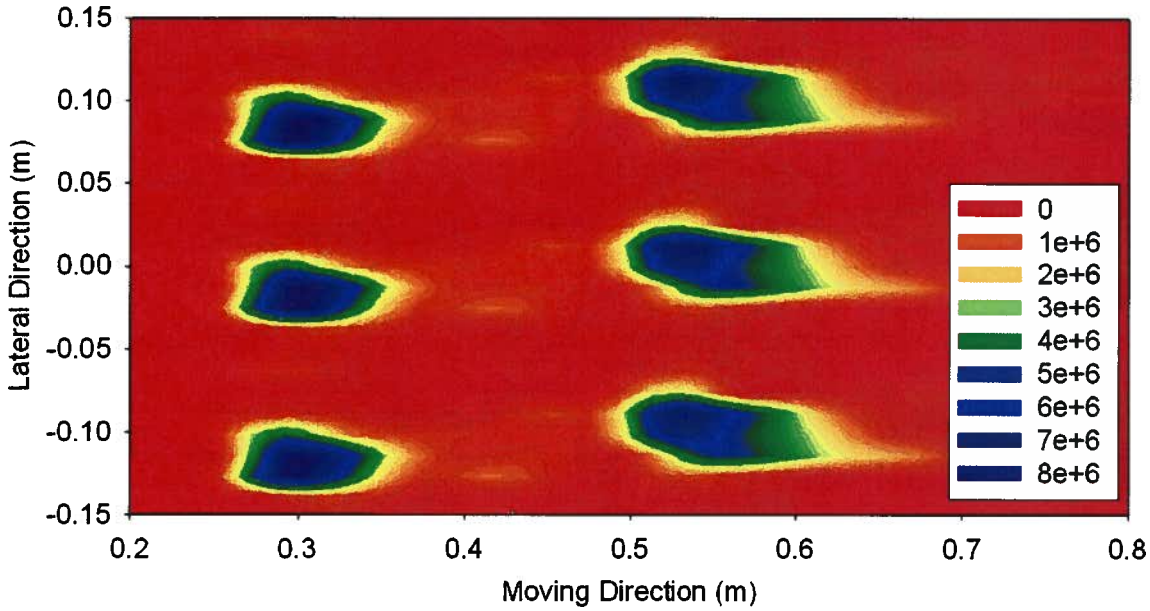

Figure 5-14 Contour plot showing surface heat flux (W/m^2) in a partially staggered nozzle configuration with an entry temperature of 350 °C

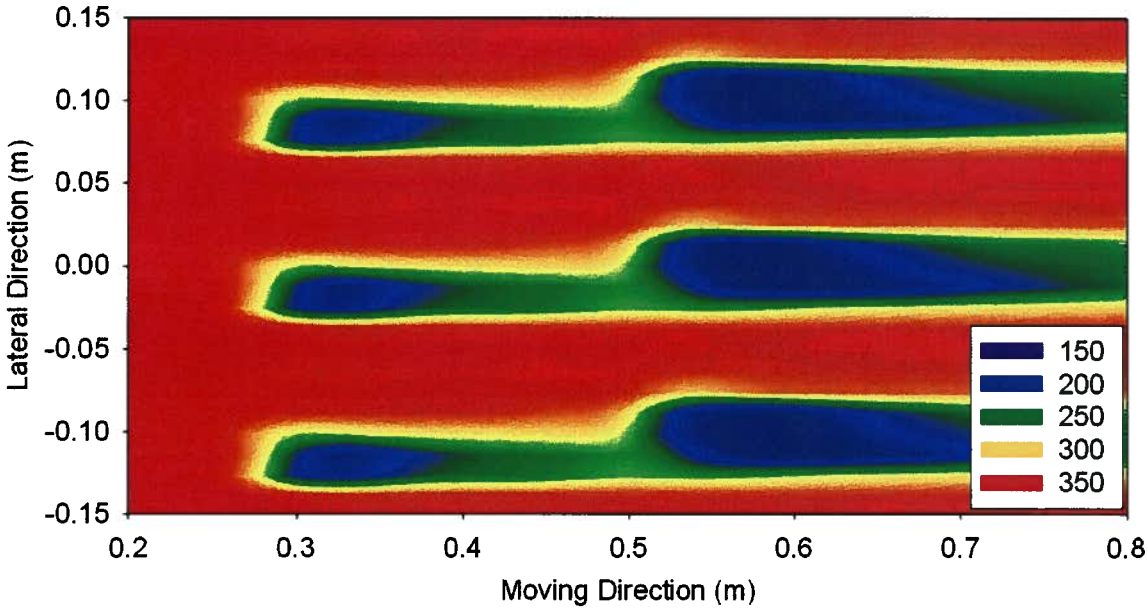

Figure 5-15 Contour plot showing surface temperature (°C) in a partially staggered nozzle configuration with an entry temperature of 350 °C

From the figures above, it can be concluded that impingement zones of the second jet line is larger than the impingement zones of the first jet line. This observation is particularly more evident in the surface temperature contour plot (Figure 5-15). This is believed to be due to the colder surface temperature in the wake of the first jet line. Since the impingement zone of the second jet line overlaps this colder zone, the water is able to readily wet this area as well, producing an enlarged foot print. Since there are different entry temperatures, the heat fluxes observed are also different and correspond to its respective entry temperature. Looking at the impingement zones of the second jet line, the area in the wake of the first jet line recorded lower heat fluxes. In the areas of the impingement zones not previously impinged, the heat fluxes observed are the same magnitude as those in the impingement zones of the first jet line.

In general, as the entry temperature decreases, the size of the impingement zone increases. This size increase appears to be dictated by the surface temperature of the to-be-impinged surface, and its distance from the stagnation line. In the impingement zones, the magnitude of the heat fluxes follows a typical boiling curve trend as a function of entry-temperature (see Figure 5-7). In a multi-jet line system, nozzle placement in a prior jet line affects the cooling conditions in a subsequent jet line by dictating the entry temperatures for the latter jet line.

To demonstrate the strong dependence of the observed cooling effect on entry temperature and distance from stagnation, the peak heat flux values at different distances from stagnation are presented as a function of temperature in Figure 5-16. Data from tests done with full (50.8 mm), partial (25.4 mm) and no stagger, and both jet line spacing

(25.4 cm and 50.8 cm) configurations are used in the plot. All tests had a plate speed of 1 m/s.

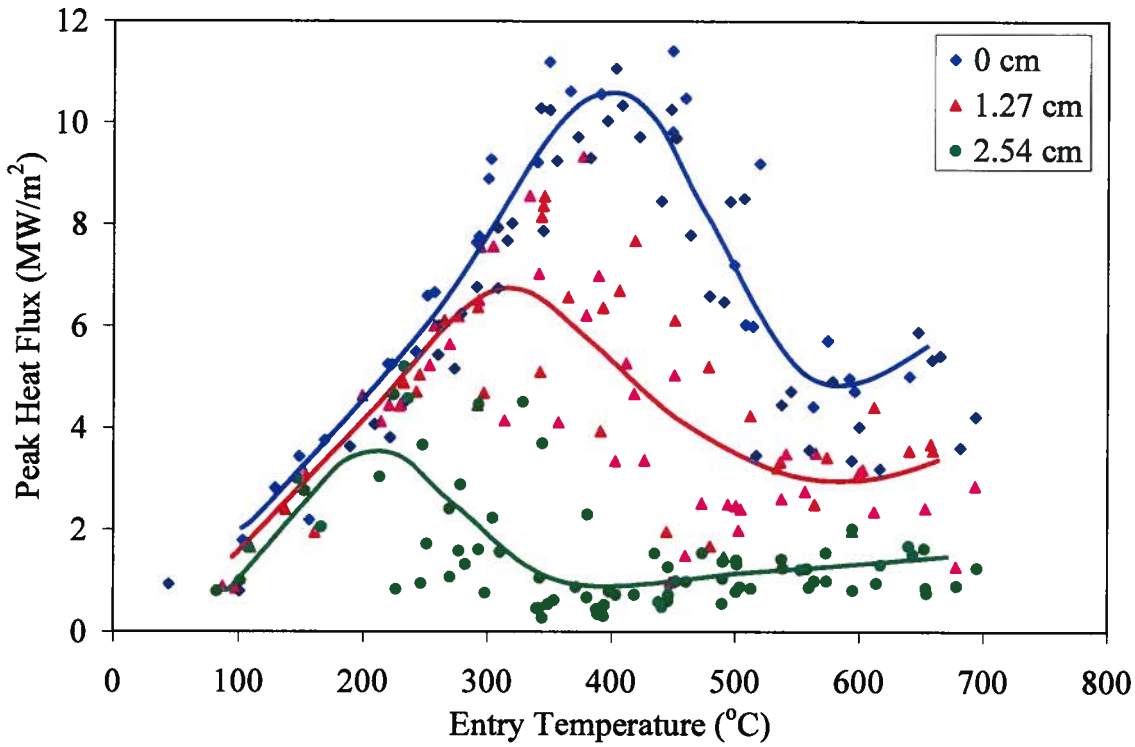

Figure 5-16 Peak heat flux values at different distances from stagnation as a function of entry temperature

Figure 5-16 shows three distinct trends corresponding to the three different distances (0, 1.27 and 2.54 cm) from stagnation. Although there is a large degree of scatter, particularly at the 2 distances outside of stagnation, there is clear separation between the three sets of data. The scatter is believed to be a result of two phenomena. First, the nature of a moving experiment gives very little time for measurement as the impingement zone passes through a thermocouple. Much of the scatter is observed in the negatively sloped portion of the curves, typically noted as the transition boiling regime. Since during transition boiling, conditions may oscillate between wet and dry, the scatter

may be a representation of the instability commonly observed during this boiling phase. Second, it has been found that the chain drive system does not traverse the plate in the same line of motion during tests and that the carrier may move sideways by as much as 5 mm. As such, the true location of the stagnation may shift from pass to pass, further compounding the oscillation between wet and dry during transition boiling. This mechanism,, however, does not affect measurements in the impingement zone as this region is much larger than the sideway movement of the carrier. Consequently, the corresponding thermocouple underneath impingement is guaranteed to remain in this zone. However, the true distance of the other thermocouples in the interaction region with respect to the location of the stagnation point becomes inaccurate.

Regardless of these issues, the plot in Figure 5-16 shows the strong dependence of the cooling effect on both entry temperature and distance from stagnation. It also shows the growth of the fully-wetted region as a function of both entry temperature and distance from stagnation. At stagnation, the peak indicates the start of fully nucleate boiling. Away from stagnation, the expansion of the wetted zone may only be possible once nucleate boiling regime is reached. Using the peaks as an indication for the start of the nucleate boiling regime, at about 320 ^{o}C and 200 ^{o}C, the fully wetted zone grows to encompass 1.27 cm and 2.54 cm away from the stagnation, respectively. The plot also shows that cooling tends to be higher and even inside the fully-wetted regions.

5.4. Total Extracted Heat

5.4.1. Analysis Approach

The previous work of Johndale [38] utilized peak heat flux values from each pass to describe the cooling phenomena that occurs. However, this method uses only one data point from a particular pass. As a result, other phenomena that may affect the data curve such as pooling of water are not aptly considered. Another technique to analyze the data is to integrate the heat flux data curve over time during a pass. Using this method to analyze the heat flux data is first reported in the experimental work of Chan [43]. Integration of the curve will utilize all the data points that are pertinent during the pass, and hence incorporate all phenomena that occur. This interpreted value is then a more representative characterization of the trends that are observed. This also eliminates variability in the analysis that may result when only one data point is used.

In order to perform the integration, a means to mark the start and end of the pass must be developed and held consistent throughout the study. Figure 5-17 presents an example of the heat flux history during pass # 7 when the jet line spacing is 25.4 mm without stagger and the plate speed is 1 m/s. The pass occurs at an entry temperature of 300 °C. The beginning of a pass is marked by the point in time when all 9 thermocouples locations report a heat flux value exceeding 0.05 MW/m^2. A value of 0.05 MW/m^2 is used because in between passes, data noise tends to oscillate below this value and will certainly be exceeded during a pass. To mark the end of the pass, the plate velocity is used to calculate the point in time wherein the thermocouple locations will traverse the distance of two jet line spacings. In essence, the end of the pass is the point in time where the thermocouple locations are just about to pass through a third jet line had there

been one. This time t_{pass} is derived using the plate speed v_{plate} and the jet line spacing $l_{spacing}$ as shown by:

$$t_{pass} = 2l_{spacing}/v_{plate} \qquad 5\text{-}1$$

For the example shown in Figure 5-17, the end of the pass is marked at 0.5 s after the beginning of the pass. The median of the two boundaries essentially bisects the first jet line from the second. Integration is accomplished by approximating the area under the curve using the trapezoidal rule. The resulting value for the example shown in Figure 5-17 is 1.1878 MJ/m^2.

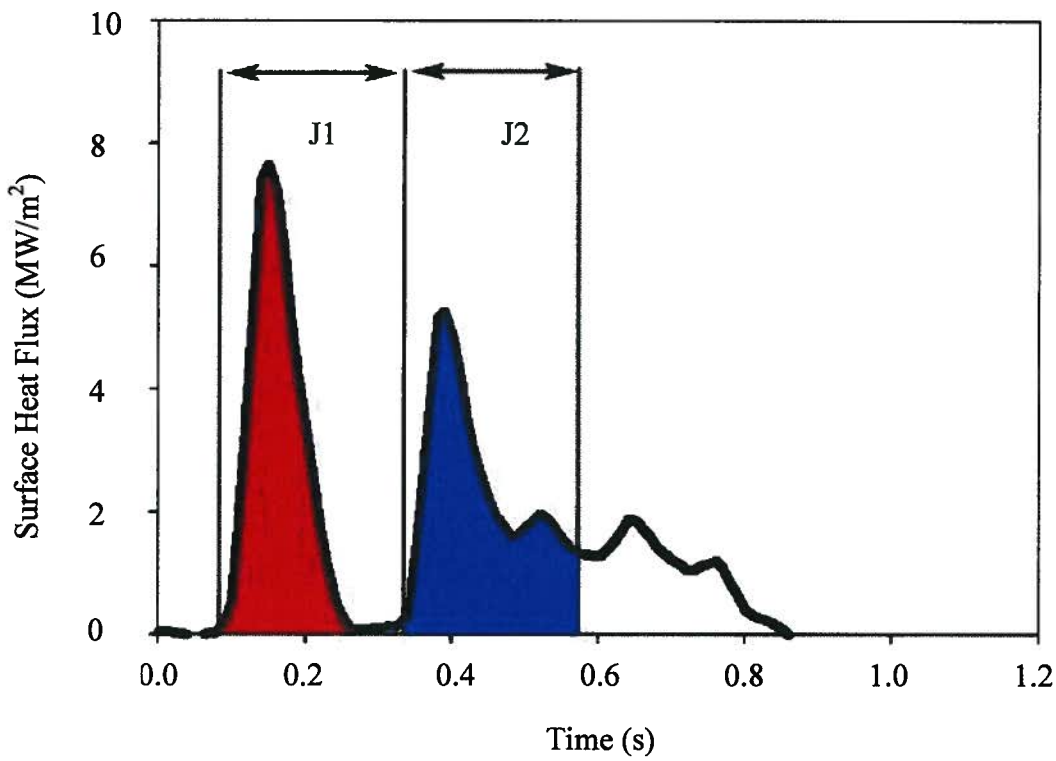

Figure 5-17 Surface heat flux during one pass with coloured regions showing integration boundaries

As a means to compare the different nozzle configurations, the overall heat extraction over the surface area of the plate is quantified by further integration with

respect to the lateral and moving directions of the plate. The procedure is similar to the integration steps previously explained, only this time, the results from each thermocouple location are utilized. Figure 5-18 shows the results of the first integration step for each thermocouple location for the same test conditions as Figure 5-17.

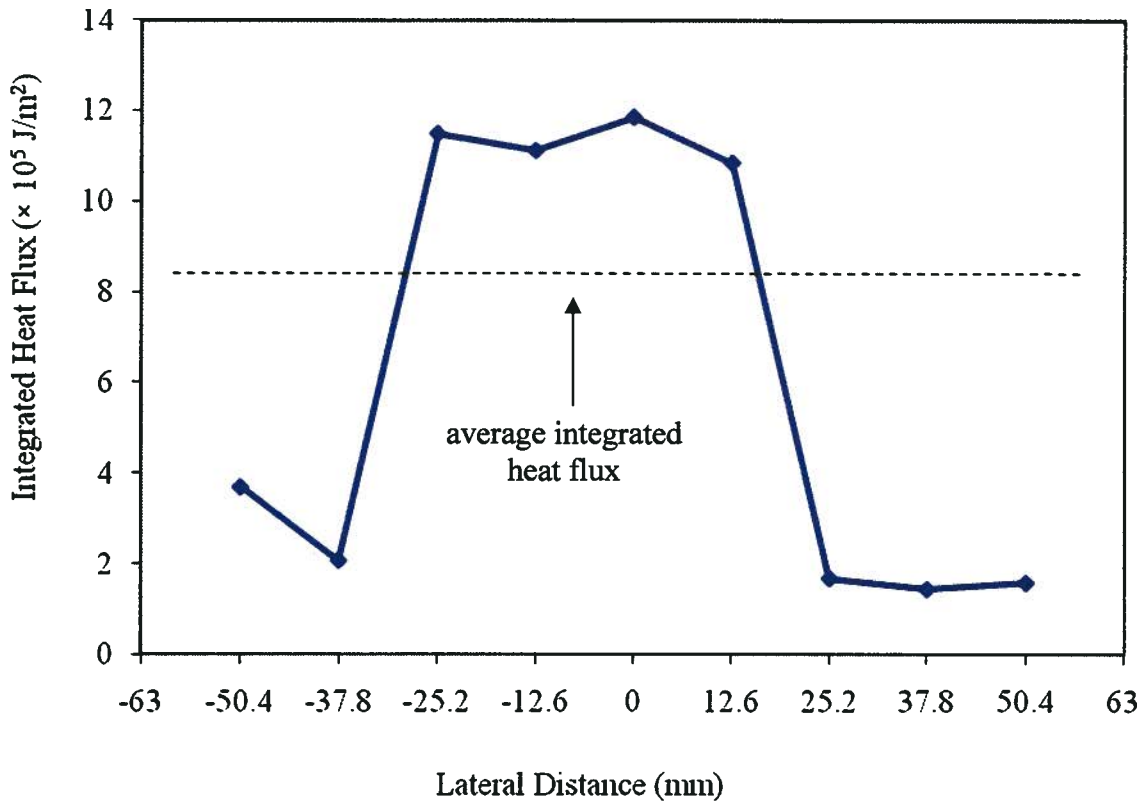

Figure 5-18 Results of first integration step for all thermocouple locations

Likewise, the integral with respect to the lateral dimension can be approximated by calculating the area under the curve using the trapezoidal rule. Studies by Chan [43] showed that different locations along the distance of the moving plate experience the same cooling phenomena albeit at different times depending on its location with respect to the impinging jet. Consequently, to obtain the total heat extracted along the plate, the

integrated heat flux across the considered plate width has to be multiplied by its length. The resulting value of all the integrations steps is the total energy extracted over the area spanned by the 9 thermocouples and the length of the plate.

5.4.2. Effect of Speed

The effect of speed on the overall heat extraction is presented in Figure 5-19. In these results, the jet line spacing is maintained at 25.4 cm and results from all stagger configurations are included. As also observed in previous studies [2, 37, 38, 43], higher heat extraction is attained at lower speeds. This observation is expected as at three times the speed, the faster moving plates will have three times less residence time under the cooling section. Apart from this difference in magnitude, the peaks of the plots tend to shift to lower temperatures with higher speeds. At 0.35 m/s, the peak of the curve is observed at 350 °C, whereas at 1.0 m/s, the corresponding peak is observed at 250 °C. With only two speeds tested, a conclusion cannot be made on the type of relationship between speed and heat extraction.

Further, the 1 m/s plot reaches its maximum at a lower surface entry temperature than that observed in the plot of peak heat flux versus entry temperature shown in Figure 5-7. This discrepancy is due to the fact that the total heat extracted values are able to take into account the effects of water pooling. As such, below an entry temperature of 350 °C, more heat is extracted even though the peak heat flux value recorded has decreased from previous passes.

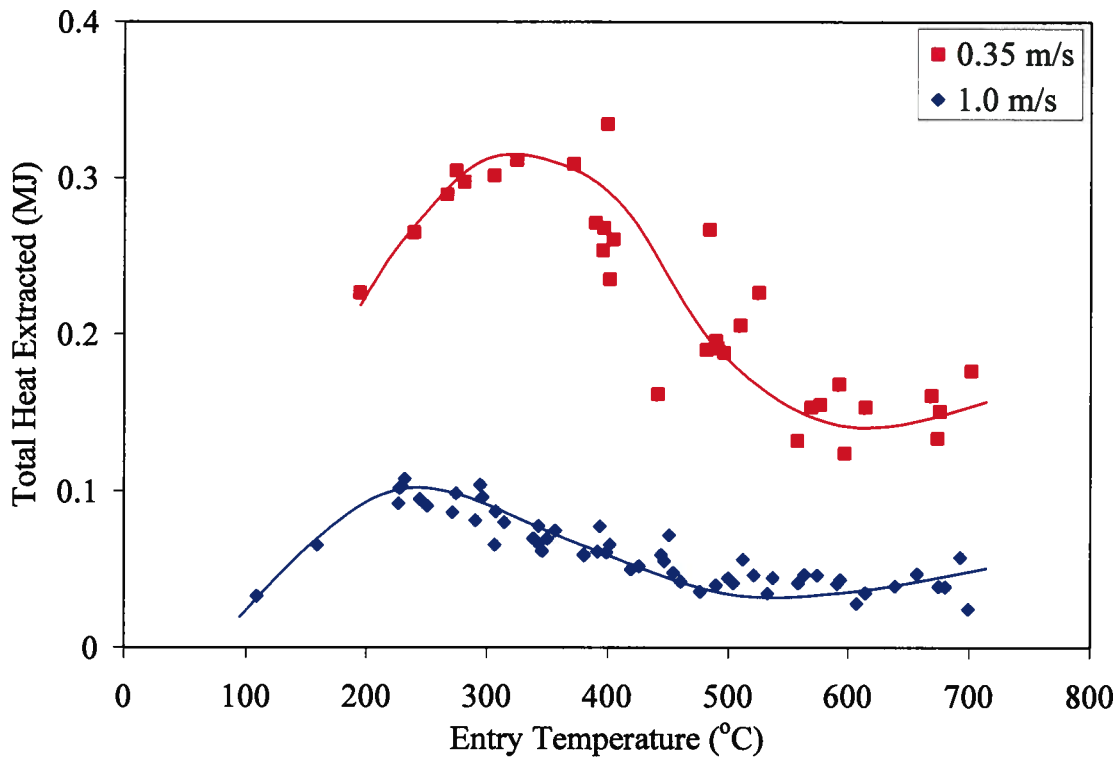

Figure 5-19 Total heat extracted for different plate speeds as a function of entry temperature

Although slower speeds produce higher heat extracted values per pass, its effective cooling rate may be hampered by the fact that slower moving plates take more time to traverse through multiple jet lines. Hence, the effective cooling rate for the different speeds is calculated by dividing the total heat extracted values by the time required for the plate to move through the jet lines. This effective time t_{eff} is derived using the plate speed v_{plate} and the length of the plate l_{plate} as shown by:

$$t_{eff} = l_{plate}/v_{plate} \qquad 5\text{-}2$$

A plot of the effective heat extraction rate as a function of surface entry temperature for the speeds tested is presented in Figure 5-20. The plot shows that the discrepancy between the two speeds is considerably less than in Figure 5-19. However, slower

moving plates are still more efficient in cooling the plate, particularly at entry temperatures above 300 °C. At lower entry temperatures, the curves for both speeds appear to follow the same trend.

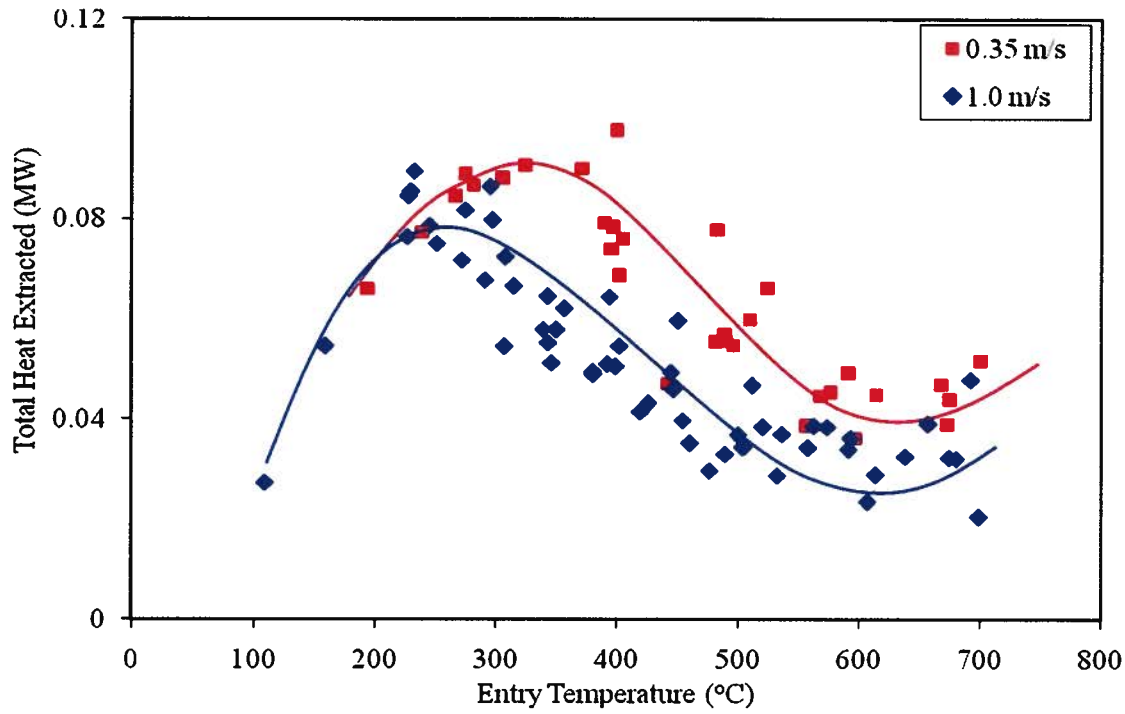

Figure 5-20 Effective heat extraction rate for different plate speeds as a function of entry temperature

5.4.3. Effect of Jet Line Spacing

The effect of jet line spacing on the cooling efficiency is depicted using the calculated heat extracted values that are plotted versus the entry temperature in Figure 5-21. These results were taken from all experiments with a plate speed of 1.0 m/s and all stagger configurations.

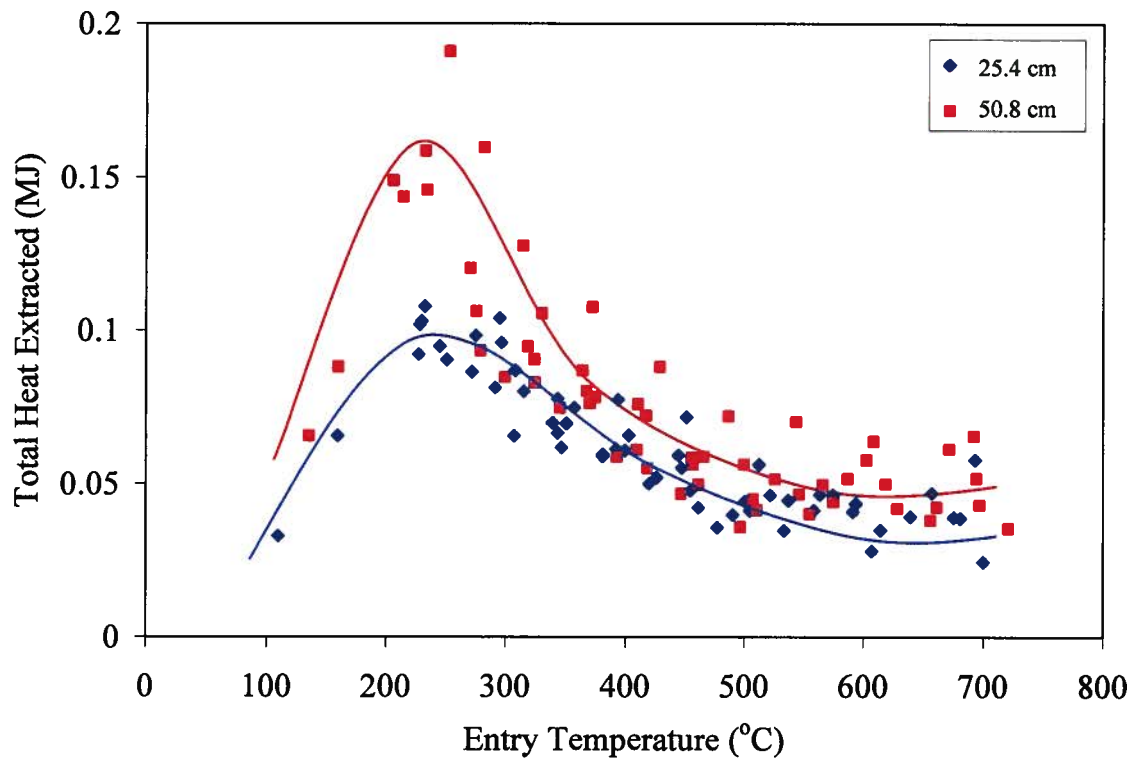

Figure 5-21 Total heat extracted for different jet line spacings as a function of entry temperature

From the above plot, it can be discerned that the trend for a jet line spacing of 50.8 cm produces higher total heat extracted values than those recorded for a jet line spacing of 25.4 cm. This discrepancy is more evident in the region of peak heat extracted, where the total heat extracted for a spacing of 50.8 cm is as much as double the values observed from a spacing of 25.4 cm. However, it should be noted that in the calculation steps explained previously, the boundaries of integration are determined by the jet line spacing used. Since the boundaries of the integration steps are much larger for a wider spacing, more of the noise is contributing to the integrated value. Also, when pooling occurs, the cooling phenomena observed as a result of impinging jets is extended until the next set of jet lines is reached by the moving plate. Hence, at progressively

lower temperatures, the discrepancy between the jet line spacings tested is larger since the cooling extension noted increases with jet line spacing.

However, with narrower jet line spacing, one can fit more jet lines along the same length than one would when using wider jet line spacing. For the jet line spacings tested, one can use 3 jet lines 25.4 cm apart to cover the same plate length as 2 jet lines 50.8 cm apart. Hence, the previously used method (Figure 5-20) is not an ideal way to compare the effects of different jet line spacing on cooling efficiency. To properly compare the cooling efficiencies of the different jet line spacings, the data is normalized by dividing by the jet line spacing. This yields a value for the total heat extracted per unit length of spacing (J/m). The result of this analysis is presented in Figure 5-22.

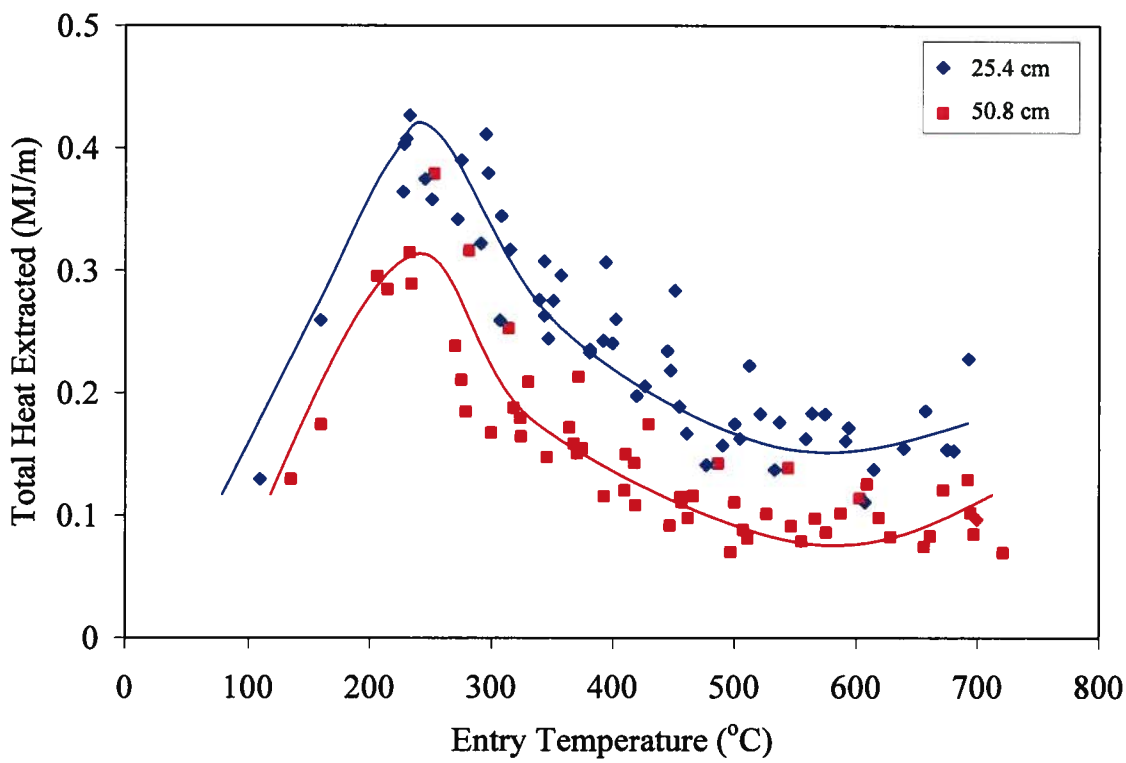

Figure 5-22 Total heat extracted per unit length of jet line spacing as a function of entry temperature

The normalized results show that the narrower jet line spacing (25.4 cm) extracts more heat per unit length of jet line spacing than the wider jet line spacing (50.8 cm). This suggests that even though the cooling effect is extended in between jet lines, particularly at lower temperatures when pooling occurs, and that this cooling extension increases with jet line spacing, the improvement is still not enough to match the cooling efficiency of having closer-spaced jet lines. At higher temperatures, the narrow jet line spacing extracts as much as 100% more than the wider jet line spacing. This difference is reduced to about 30% in the region of peak heat extraction, due the aforementioned pooling effects.

5.4.4. Effect of Stagger

A plot of the total heat extracted versus entry temperature for the different stagger positions is presented in Figure 5-23. In these results, plate speed and jet line spacing are held the same at 1.0 m/s and 25.4 cm, respectively.

As seen in Figure 5-23, all stagger configurations generate the same trends indicating that essentially equal amounts of heat are being extracted throughout the temperature range of run-out table cooling. Referring back to the contour plots in Figures 5-10 to 5-13, the plots without stagger (Figures 5-10 and 5-11) depict alternating layers of high and low heat extraction. On the other hand, the plots with full stagger (Figures 5-12 and 5-13) depict a more homogeneous heat extraction. The heat extraction with full stagger is generally not as intense as along the stagnation lines of the case without stagger. However, this lower heat extraction is more spread out over the surface area of

the plate. Hence, the total heat extracted over similar areas covered by non-staggered and fully staggered nozzle configurations end up being the same.

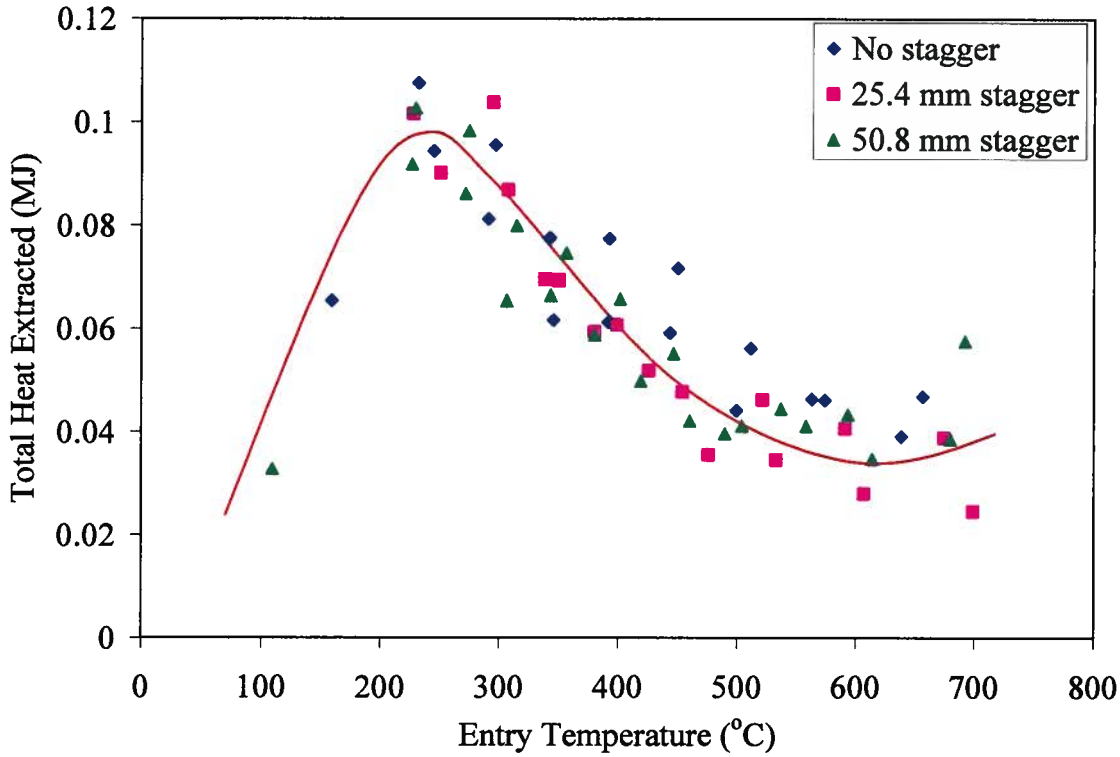

Figure 5-23 Total heat extracted for different nozzle stagger configurations as a function of entry temperature

To further demonstrate the similar heat extraction by different stagger configurations, the average post-pass temperature is plotted as a function of the average entry temperature as shown in Figure 5-24. Results are from tests with plate speed and jet line spacing of 1.0 m/s and 25.4 cm, respectively.

The average post-pass temperature is the average of the surface temperatures from each thermocouple location 0.25 seconds after the pass. The difference between the average entry and post-pass surface temperatures is proportional to the energy lost by the plate. As shown in the plot, data from no stagger, 25.4 mm stagger and 50.8 mm stagger

follow the same trend. This suggests that the average temperature drop, and hence energy extracted are the same for the stagger configurations tested.

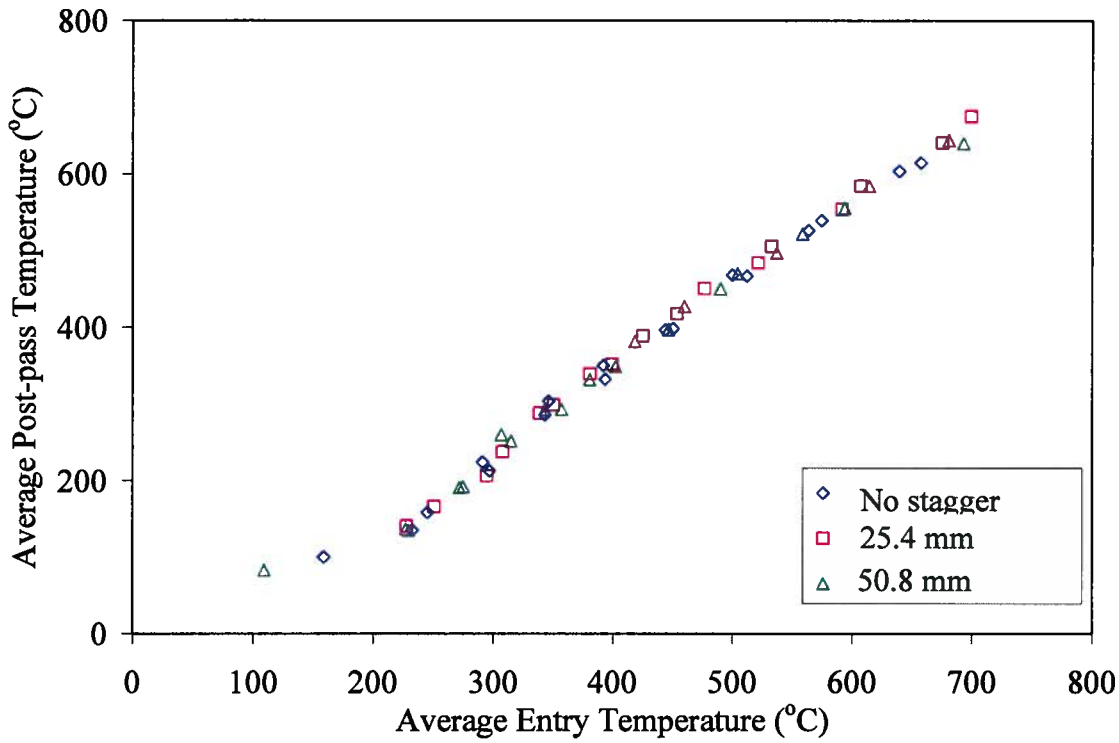

Figure 5-24 Plot of the average post-pass temperature versus average entry temperature

5.5. Temperature Gradients

An important information to asses microstructure variation and thermal stresses in the plate is the difference in the surface temperature gradient along the transverse direction for the different nozzle configurations. Larger gradients are obtained in the case of no stagger, as shown by the "banding" formation of hot and cold regions depicted in Figure 5-9 and Figure 5-12, respectively. Although some "banding" can also be observed

in Figure 5-13 for the fully staggered nozzle arrangement, it is considerably less pronounced.

The surface temperature gradient is quantified and presented in Figure 5-25 as a function of the entry temperature. The calculated gradient represents the standard deviation (σ_T) of the surface temperatures at all nine thermocouple locations 0.25 seconds after passing under the second jet line (post-pass). The standard deviation is a measure of the spread of values with respect to its arithmetic mean, i.e. the average post-pass surface temperature, and is calculated as follows:

$$\sigma_T = \sqrt{\frac{1}{N}\sum_{i=1}^{N}\left(T_{0.25,i} - T_{0.25,Avg}\right)^2} \qquad 5\text{-}3$$

, where N is the population of the data set (thermocouple locations), $T_{0.25}$ is the post-pass surface temperature and $T_{0.25,Avg}$ is the arithmetic mean of the post-pass surface temperatures.

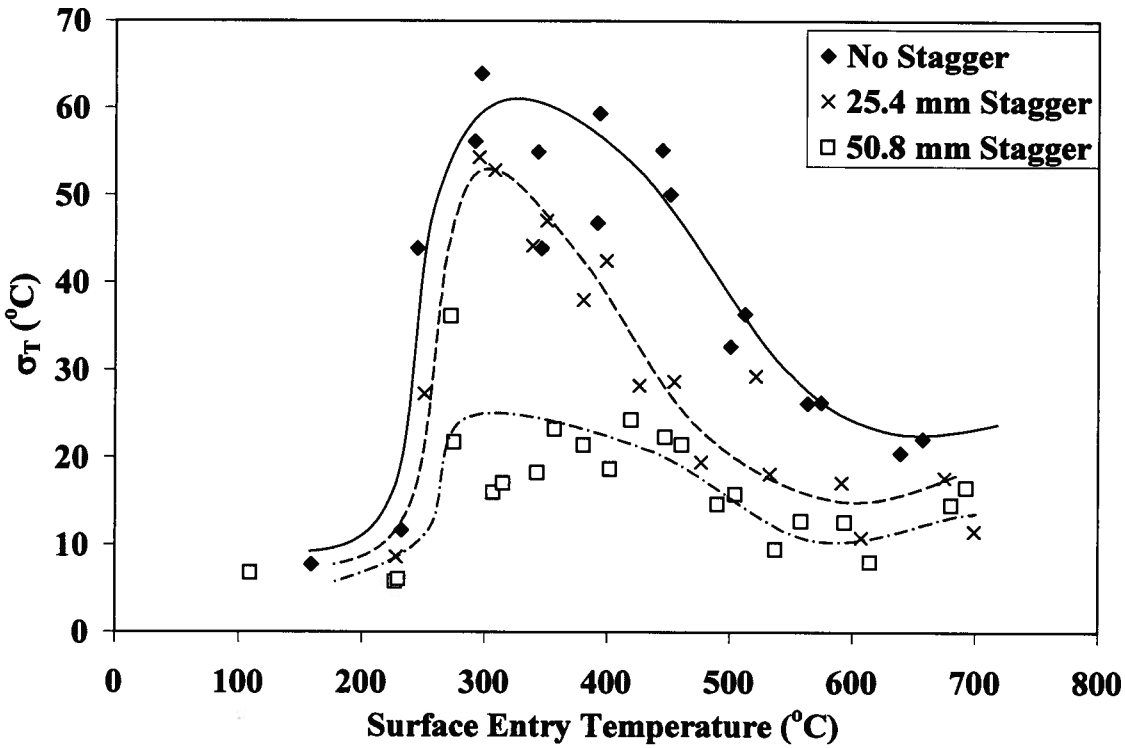

Figure 5-25 Plot of the surface temperature standard deviation (σ_T) with respect to pass entry temperature

As can be seen in Figure 5-25, the lower standard deviation observed in the fully staggered case suggests less scatter of the surface temperature data, indicating a more uniform cooling. In all cases, the largest temperature gradients occur at surface entry temperatures in the range of 300 °C to 450 °C, i.e. the range where the highest peak heat fluxes are observed (see Figure 5-7). This observation is consistent with the fact that higher heat extraction provides the potential for increased temperature gradients across the plate. At sufficienly low temperatures (< 250 °C), similar temperature spreads are observed in all cases. This suggests that the highly wetted zone has grown to cover a larger area and that uniform cooling is observed, regardless of nozzle configuration.

6. CONCLUSION

6.1. Summary

Multiple top jet cooling experiments on a hot moving steel plate have been carried out at a pilot-scale run-out table facility. The stagger between nozzles, jet line spacing and plate speed are systematically varied to investigate their effects on the cooling of hot moving steel plates. Sub-surface temperature histories are measured during experiments and are used to generate surface temperature and heat flux histories using IHC analysis. Using the calculated surface temperature and heat flux histories, contour plots depicting the different cooling regions at different passes are generated. Also, the surface heat flux histories are integrated with respect to time and space to quantify the total heat extracted and to compare the cooling efficiencies of the different nozzle configurations and plate speeds.

The results show that for the conditions studied, the cooling efficiency is unaffected by nozzle stagger as long as plate speed, jet line spacing and flow rate are the same. However, uniformity of cooling is dependent on the locations and distribution of jet impingement. A fully staggered nozzle arrangements leads to more uniform cooling. At entry temperatures below 250 °C, the impingement zone grows to cover a wide surface area, such that the cooling attained is uniform regardless of nozzle stagger configuration.

It has also been shown that regardless of nozzle configuration, the fully-wetted regions appear to expand similarly with decreasing temperature. This, however, is only based on the test conditions used, wherein significant pooling does not occur in between jet lines. Such observations may prove different when higher water flow, for example,

are used. Nonetheless, it has been found that the cooling experienced by a local area generally relies on its location with respect to the stagnation line, and its temperature prior to the pass. Thus, the aforementioned parameters can be utilized to predict the cooling that will take place and to map the areas that will be fully-wetted. Such information is useful in modeling the heat transfer processes occurring during runout table cooling, and as well as optimizing nozzle configuration to ensure high cooling efficiency without compromising cooling uniformity. Ideally, the nozzles should be configured such that the entire width of the plate is fully wetted either through proper spacing between nozzles or proper staggering between jet lines.

The results also show a dependence of cooling efficiency on plate speed and jet line spacing. Slower moving plates tend to have higher residence time under the water jets, and thus higher heat fluxes and total heat extracted are obtained. Even when the amount of time required to move a plate through the jet lines is considered, slower speeds still produced higher effective cooling rates. On the other hand, longer distances between jet lines produces higher heat extracted values per pass. However, shorter distances between jet lines are found to extract more heat per unit length of jet line spacing and are deemed more effective.

6.2. Recommended Future Work

In light of the findings of this study, the following recommendations are suggested for future work:

1. Systematically varying flow rate to quantify its effect on cooling efficiency. In addition, higher flow rates may introduce a dependence of

cooling on jet line spacing as the expected increase in water pooling may affect the heat extraction observed in subsequent jet lines.

2. Testing with plate speeds in excess of 1.0 m/s, and between 0.35 and 1.0 m/s. This will provide a better means to correlate the effect of speed on cooling, which can potentially be extrapolated to speeds observed in actual run-out tables. Similarly to the first point, higher speeds may also introduce a dependence of cooling on jet line spacing as there will be less residence time in between jet lines for the water to fully evaporate or flow away from the impingement zones.
3. Introducing more thermocouples particularly in the areas surrounding the expected stagnation line. By having data at closer intervals, a better approximation of the integral with respect to the lateral dimension of the plate can be made. Also, the evolution of the fully-wetted region can be better tracked and quantified. Better correlations can be made with regards to the effect of entry temperature and distance from stagnation on the subsequent cooling effect. However, further study in this area will also necessitate better control of plate position during experiments. This will allow more accurate measurement of distances with respect to the expected stagnation points.

REFERENCES

1. Clay D.B. et al. *Development of Line Pipe Steels*. Philosophical Transactions of the Royal Society of London. Series A, Mathematical and Physical Sciences. 282: pp. 305-318, July 1976.
2. Prodanovic V., Fraser D., Militzer M., *Simulation of Runout Table Cooling by Water Jet Impingement on Moving Plates - A Novel Experimental Method.* in *2nd International Conference on Thermomechanical Processing of Steel.*, p. 25-32, ed. M. Lamberights, Belgium, July 2004.
3. Liu Z.H., Wang J., *Study on Film Boiling Heat Transfer for Water Jet Impinging on High Temperature Flat Plate.* International Journal of Heat and Mass Transfer, 2001. 44: p. 2475-2481.
4. Militzer M., Hawbolt E.B., Meadowcroft T.R., *Microstructural Model for Hot Strip Rolling of High-Strength-Low-Alloy Steels.* Metallurgical and Materials Transactions A, 2000. 31A: p. 1247-1259.
5. Chester, N., *A Study of Boiling Heat Transfer on a Hot Steel Plate Cooled by an Inclined Circular Bottom Water Jet, M.A.Sc. Thesis*. 2006, University of British Columbia, Vancouver.
6. Tacke G., Litzke H., Raquet E., *Investigations into the Efficiency of Cooling Systems for Wide-Strip Hot Rolling Mills and Computer-Aided Control of Strip Cooling.* in *Accelerated Cooling of Steel.*, p. 35-54, Pittsburgh, Pennsylvania.
7. Kohring F.C., *WATERWALL Water-Cooling Systems.* Iron and Steel Engineer, 1985. 62(6): p. 30-36.

8. Han F.; Chen S.J.; Chang C.C., *Effect of surface motion on liquid jet impingement heat transfer*, American Society of Mechanical Engineers, Heat Transfer Division, (Publication) HTD, v 180, Fundamentals of Forced and Mixed Convection and Transport Phenomena, 1991, p 73-81.

9. Zumbrunnen D.A., Viskanta R., Incropera F.P., *The Effect of Surface Motion on Forced Convection Film Boiling Heat Transfer.* Journal of Heat Transfer, 1989. 111: p. 760-766.

10. Chen S.J., Tseng A.A., *Spray and Jet Cooling in Steel Rolling.* International Journal of Heat and Fluid Flow, 1992. 13(4): p. 358-369.

11. Nukiyama S., *The Maximum and Minimum Values of Heat Transmitted from Metal to Boiling Water Under Atmospheric Pressure (English Translation)*, International Journal of Heat and Mass Transfer, Vol. 9, Issue 12, 1966, 1419-1433.

12. Drew T.B., Mueller C., *Boiling*, Transactions of the American Institute of Chemical Engineers, Vol 33, 1937, 449-471.

13. Wolf D.H., Incropera F.P., Viskanta R., *Jet Impingement Boiling.* Advances in Heat Transfer, 1993. 23: p. 1-131.

14. Robidou H., Auracher H., Gardin P., Lebouche M., *Controlled Cooling of a Hot Plate with a Water Jet.* Experimental Thermal and Fluid Science, 2002. 26: p. 123-129.

15. Wolf D.H., Incropera F.P., Viskanta R., *Local Jet Impingement Boiling Heat Transfer.* International Journal of Heat and Mass Transfer, 1996. 39(7): p. 1395-1406.

16. Hauksson A., *Experimental Study of Boiling Heat Transfer During Water Jet Impingement on a Hot Steel Plate, M.A.Sc. Thesis.* 2001, University of British Columbia, Vancouver.

17. Miyasaka Y., Inada S., Owase Y., 1980, *Critical heat flux and subcooled nucleate boiling in transient region between a two-dimensional water jet and a heated surface*, J. Chemical Engineering of Japan, 13(1): 29-35.

18. Liu Z.H., Tong T.F., Qiu Y.H., *Critical Heat Flux of Steady Boiling for Subcooled Water Jet Impingement on the Flat Stagnation Zone.* Journal of Heat Transfer, 2004. 126: p. 179-183.l

19. Liu Z.H., Zhu Q.Z., *Prediction of Critical Heat Flux for Convective Boiling of Saturated Water Jet Impingement on the Stagnation Zone.* Journal of Heat Transfer, 2002. 124: p. 1125-1130.

20. Mitsutake Y., Monde M., *Ultra High Critical Hat Flux During Forced Flow Boiling Heat Transfer with an Impinging Jet.* Journal of Heat Transfer, 2003. 125: p. 1038-1045.

21. Hammad J., Mitsutake Y., Monde M., *Movement of Maximum Heat Flux and Wetting Front During Quenching of Hot Cylindrical Blocks.* International Journal of Thermal Science, 2004. 43: p. 743-752.

22. Pan C., Hwang J.Y., Lin T.L., *The Mechanism of Heat Transfer in Transition Boiling.* International Journal of Heat and Mass Transfer, 1989. 32(7): p. 1337-1349.

23. Ishigai S., N.S., Ochi T. *Boiling Heat Transfer for a Plane Water Jet Impinging on a Hot Surface.* in *Proceedings of the 6th International Heat Transfer Conference.*, p. 445-450, Hemisphere, Toronto, Canada, 1978.

24. Liu Z.H., *Prediction of Minimum Heat Flux for Water Jet Boiling on a Hot Plate.* Journal of Thermophysics and Heat Transfer, 2003. **17**(2): p. 159-165.

25. Filipovic J., Viskanta R., Incropera F.P., Veslocki T.A., *Cooling of a Moving Steel Strip by an Array of Round Jets*, Steel Research, 65, 541-547, 1994.

26. Monde M., *Burnout heat flux in saturated forced convection boiling with an impinging jet*, Heat Transfer Japanese Res., 9(1), 1980, pp31-41.

27. Sakhuja R.K.; Lazgin F. S.; Oven M. J. *Boiling heat transfer with arrays of impinging jets*, ASME Paper No. 80-HT-47, 1980.

28. Slayzak S.J., Viskanta R., Incropera F. P., *Effects of Interaction between Adjacent Free Surface Planar Jets on Local Heat Transfer from the Impingement Surface*, Int. J. Heat and Mass Transfer, Vol. 37, No. 2, 1994, pp. 269-282.

29. Slayzak S.J., Viskanta R., Incropera F.P., *Effects of Interactions between Adjoining Rows of Circular, Free-Surface Jets on Local Heat Transfer from the Impingement Surface*, Journal of Heat Transfer, Vol. 116, February, 1994, pp. 88-95.

30. Harahuchi Y., Hariki M., *Analysis of heat transfer of laminar cooling for uniform temperature control in hot strip mill*, 2nd Intl. Conf. On Modelling of Metal Rolling Processes, (ed. By JH Beynon et al), 9-11, Dec., 1996, London, UK, pp606-611.

31. Liu, Z.D., *Experiments and Mathematical Modelling of Controlled Runout Table Cooling in a Hot Rolling Mill, Ph.D. Thesis*. 2001, University of British Columbia, Vancouver.

32. Zumbrunnen D.A., Incropera F.P., Viskanta R., *Method and Apparatus for Measuring Heat Transfer Distributions on Moving and Stationary Plates Cooled by a Planar Liquid Jet.* Experimental Thermal and Fluid Science, 1990. 3(2): p. 202-213.

33. Hatta N., Osakabe H, *Numerical Modelling for Cooling Process of a Moving Hot Plate by Laminar Water Curtain*, ISIJ International, Vol. 29, No. 11, 1989, pp.919-925.

34. Chen S.J., Tseng A.A., Han F., *Spray and Jet Cooling in Steel Rolling*, Heat Transfer in Metals and Containerless processing and Manufacturing, ASME 1991, Vol. 162, p 1-11

35. Chen S.J., Kothari J., *Temperature distribution and heat transfer of a moving metal strip cooled by a water jet*, American Society of Mechanical Engineers (Paper), 1988, WA/NE4 8p

36. Chen S.J., Kothari J., Tseng A.A., *Cooling of a moving plate with an impinging circular water jet*, Experimental Thermal and Fluid Science, v 4, n 3, May, 1991, p 343-353

37. Prodanovic V., Militzer M., *Runout Table Cooling Simulation for Advanced Linepipe Steels*. in *Pipeline for the 21st Century - The Metallurgical Society of CIM*. 2005. p. 127-142, Montreal,Canada.

38. Jondhale, K., *Heat Transfer During Multiple Jet Impingement on the Top Surface of Hot Rolled Steel Strip, M.A.Sc. Thesis*. 2007, University of British Columbia, Vancouver.

39. Zhang, P., *Study of Boiling Heat Transfer on a Stationary Downward Facing Hot Steel Plate Cooled by a Circular Waterjet, M.A.Sc Thesis*. 2004, University of British Columbia, Vancouver.

40. Boyer H.E. and Gall T.L., *Metals handbook desk edition*, American society of metals, 1995.

41. Caron, E., Wells, M.A., and Li, D., *A compensation method for the disturbance in the temperature field caused by sub-surface thermocouples*, Metallurgical And Materials Trans. B, 2005 37, 475-483

42. Li D., Wells M.A., *Effect of Subsurface Thermocouple Installation on the Discrepancy of the Measured Thermal History and Predicted Surface Heat Flux During a Quench Operation.* Metallurgical and Material Transactions B, 2005 36, 343-54.

43. Chan P., *Jet Impingement Boiling Heat Transfer at Low Coiling Temperatures, M.A.Sc. Thesis*. 2007, University of British Columbia, Vancouver.